

Two-Phase Modeling of Fluid Injection Inside Subcutaneous Layer of Skin

Abdush Salam Pramanik^{*1}, Bibaswan Dey^{†1}, Timir Karmakar^{‡2}, and Kalyan Saha^{§1}

¹Department of Mathematics, University of North Bengal, Raja Rammohunpur, Darjeeling-734013, West Bengal, India

²Department of Mathematics, National Institute of Technology Meghalaya, Shillong-793003, Meghalaya, India

Abstract

The motivation of this present theoretical investigation comes from the delivery of various drugs and vaccines through subcutaneous injection (SCI) to the human body. In the SCI procedure, a medical person takes a big pinch of skin of the injection applicable area of a patient to pull the subcutaneous layer (SCL) from the underlying muscle layer to smooth the execution of the procedure. Generally, the human skin, particularly SCL, is a heterogeneous and anisotropic living material. The major constituents of the SCL are adipose cells or fat cells and interstitial fluid. These adipose cells are oriented in such a way that the hydraulic conductivity of the SCL exhibits anisotropy. Consequently, one can adopt the field equations of mixture theory to describe the continuum nature of SCL. This mathematical modeling involves a perturbation technique where the small aspect ratio of the SCL provides a valid perturb parameter. This study highlights the issue of the mechanical response of the adipose tissue in terms of the anisotropic hydraulic conductivity variation, the viscosity of the injected drug, the mean depth of subcutaneous tissue, etc. In particular, the computed stress fields can measure the intensity of pain experienced by a patient after this procedure. Also, this study discusses the biomechanical impact of the creation of one or more eddy structure(s) due to the high pressure developed, increased tissue anisotropy, fluid viscosity, etc., within the area of applying injection.

*Electronic address: rs_abdush@nbu.ac.in

†Electronic address (Corresponding Author): bibaswandey@nbu.ac.in

‡Electronic address: tkarmakar@nitm.ac.in

§Electronic address: kalyansaha@nbu.ac.in

Keywords: Subcutaneous Injection; Tissue Anisotropy; Adipose Cells; Line of Injection; Biphasic Mixture Theory; Composite Stream Function

MSC[2020] 92C10; 92C35; 92C50; 35B20; 76D05

1 Introduction

Drug injection is a popular and efficient way to deliver a drug into biological tissues in order to get more appropriate results. Among the several injection techniques, subcutaneous injection (SCI) is a useful as well as highly effective corresponding to the medication of insulin, morphine, epinephrine, hydromorphone, diacetylmorphine, goserelin, metoclopramide, heparin, fertility drugs etc. inside fatty subcutaneous tissue immediately below the dermis layer (DL) [1]. SCI becomes advantageous for possible self-administration for the patients who need particular medicine regularly [2]. Also, this technique becomes an alternative way of drug intake that results in better drug mobility for patients with poor venous access [3, 4]. In the context of safety and efficacy, the SCI is better than any other technique, such as intravenous or intramuscular injection [5, 6]. A survey done by Stoner et al. [7] suggests that the subcutaneous route is preferable to the patients as compared to the intravenous route. For those patients who need multiple daily doses of one or more drug(s), SCI provides a broader range of alternative sites of injection than intramuscular injection [8].

To understand the detailed mechanism of SCI and the corresponding mechanical response of the tissue within the area of application of injection, it is our primary goal to understand the composition of the tissue at the injection site. The subcutaneous layer (SCL) is in general a composition of adipose tissue along with extracellular fluid [9, 10, 11]. According to Shrestha and Stoeber [12, 13], skin tissue behaves as a deformable porous medium that absorbs fluid as a result of the formation of a cavity under the local expansion of tissue rather than rupturing.

The fluid flow through the tissue matrix during an intradermal injection is affected by its porosity and permeability. Hence, fluid flow and deformation of solid phases get coupled [14]. The porosity and permeability variation during an injection plays a vital role in controlling the accuracy of the amount of fluid injected into the skin at different stages of the injection [12]. Consequently, one can control the dosage of a drug to be delivered. Identifying the field equations that govern the above phenomena would be essential. In this context, one can go through the classical study of Oomens et al. [15] where skin tissue has been considered as a biphasic mixture of solid (s) and fluid (f) constituents. A set of non-linear field equations can describe the biphasic nature of skin tissue. In this context, one can go through the classical literature on field theories of mechanics for a detailed structure of governing field equations [16, 17, 18, 19, 20, 21]. For a wide range of authorship, those field equations of mixture theory are presented in some next-generation literature. In this study, we maintain adequate clarity to express the principal aspect of the modelling using the fundamental laws of mechanics, e.g., mass and momentum conservation equations. If ρ_i and \mathbf{V}_i represent

apparent mass density and velocity of i^{th} constituent ($i \in \{s, f\}$) then the mass balance equation for i^{th} constituent becomes

$$\frac{\partial \rho_i}{\partial t} + \nabla \cdot (\rho_i \mathbf{V}_i) = m_i, \quad i \in \{s, f\}, \quad (1)$$

$$\sum_{i=s,f} m_i = 0. \quad (2)$$

On the other hand, the balance of momentum for the i^{th} constituent is given by

$$\rho_i \frac{D\mathbf{V}_i}{Dt} = \nabla \cdot \mathbf{T}_i + \rho_i \mathbf{F}_i + \mathbf{\Pi}_i, \quad i \in \{s, f\}, \quad (3)$$

where $D\mathbf{V}_i/Dt = \partial/\partial t + (\nabla \cdot \mathbf{V}_i)$ denotes the material derivative, \mathbf{T}_i represents cauchy's stress tensor, \mathbf{F}_i is the external body force corresponding to the i^{th} constituent and $\mathbf{\Pi}_i$ is the interactive force on i -th constituent due to the other. In addition, the balance of momentum of the whole tissue matrix leads to

$$\sum_{i=s,f} (\mathbf{\Pi}_i + m_i \mathbf{V}_i) = 0. \quad (4)$$

Similar sets of equations (1)-(4) have been reported in several studies based on mixture theory [17, 19, 20, 21, 22, 23, 24, 25, 26]. Depending on the physical behavior, for an appropriate modelling, a tissue can be considered as mixture of two or several fluid constituents. For example, while considering growth of a tissue, one can assume the cellular phase to behave as a fluid continuum [27, 28, 29]. Therefore, the dynamics of each constituent can be governed by a similar fluid momentum equation. Each constituent can be distinguished from others in terms of viscosity [30, 22]. However, the situation would be different when flow-induced deformation of biological tissues is studied. Barry and Aldis [31] compared the flow-induced deformation between soft biological tissues and polyurethane sponge through a mathematical model assuming the solid phase to behave as a poroelastic material. In this regard, the dynamics of the whole tissues are governed by the set of equations (1)-(4) stated above. But the Cauchy stress tensor (\mathbf{T}_s) corresponding to the solid phase has to follow the stress relation for an elastic material. On the other hand, the fluid stress (\mathbf{T}_f) can depend either solely on the pore pressure [31] or both the pore pressure and fluid viscous force [32]. Note that any volumetric change in the tissue due to fluid-induced deformation is infinitesimal. Barry et al. [33] studied fluid injection as a point source into a deformable porous layer with both the boundaries impermeable to fluid flow using biphasic mixture theory. Later, Barry et al. [34] extended their study by considering a set of boundary conditions where the upper surface is permeable to fluid flow. In this context, the models of Li and Johnson [35] are relevant to the SCI of insulin. Recently, Shrestha and Stoeber [13] have introduced a semi-empirical model based on experimental data and constitutive equations of flow through biological tissue that elucidates the fluid transport through skin tissue. Injecting fluid into the skin involves a coupled interaction with the deformation of the soft porous matrix of skin tissue since skin tissue is a deformable porous medium. Their study assumes the permeability (K) of any biological tissue (particularly the skin tissue), in the following form

$K = K_0 \exp(\mathcal{M}\mathcal{E}_{ij})$. \mathcal{E}_{ij} denotes the volumetric strain in the solid matrix of skin tissue; K_0 and \mathcal{M} are macroscopic material constants. This form of permeability is general; however, other forms of permeability can also be discussed. The concept of anisotropic permeability comes when K_0 assumes a form of a square matrix, i.e., $K_0 = K_{0_{ij}}$ when ij th entry is the permeability in the ij th direction concerning the coordinate axes. For simplicity, \mathcal{M} can be chosen zero as a particular case.

Besides the composition of tissue structure, tissue hydraulic conductivity or tissue permeability plays an important role in delivering the drug through the injection. If we consider a soft biological tissue as a deformable porous media [14], it may consist either of an isotropic matrix whose permeability is the same along all directions [36, 37, 38, 39, 13], or an anisotropic matrix whose permeability varies with direction [40, 41, 42, 43]. In particular, the anisotropic permeability may varies in the principal directions only [44, 45]. The effects of anisotropic permeability have been observed in the various study of articular cartilage [46, 47, 48]. Federico and Herzog [49] studied the effects of anisotropic permeability in a biological tissue filled with interstitial fluid and reinforced by impermeable collagen fibers. Most of the previous studies are mainly based on the isotropic nature, and there are few involving the anisotropic behavior of biological tissue. But due to the variations in the distribution of collagen fibers, soft connective tissue can show anisotropic behavior [50]. SCL is a soft connective layer of tissue; it possesses anisotropic permeability. As reported by Kim et al. [1] for a fixed flow rate, vertical permeability of skin tissue is greater than horizontal permeability, and there is no strong evidence that the converse may not hold. This incident motivates us to think about the situation when the horizontal permeability is greater than the vertical permeability. Therefore in this study, we consider the anisotropic nature of the SCL in the case mentioned above, which may be an interesting topic.

A detailed literature review indicates the lacuna in mathematical modeling of fluid flow problems inside soft connective tissues, including both anisotropic and deformable nature. Consequently, this article introduces a mathematical model to discuss drug delivery through an SCI. The subcutaneous tissue region has a biphasic description of two main constituents fat adipose cells (AC) and interstitial fluid (IF). In addition, the interstitial hydraulic conductivity has anisotropic, which varies in the principal directions only. In this current study, our primary aim is to discuss the mechanical response of the SCL in terms of the variation of anisotropic hydraulic conductivity, the viscosity of the injected drug, the mean depth of the SCL, etc. In addition, we would like to study the pain realized by a patient near the injection site with the help of pressure gradient and shear stress.

2 Mathematical formulation

SCIs are typically used to administer drugs and vaccines into the fatty tissue layer (subcutaneous tissue) sandwiched between the dermis layer (DL) and muscle layer (ML). While injecting a fluid containing drugs or vaccines into a patient, the lifted skin fold technique

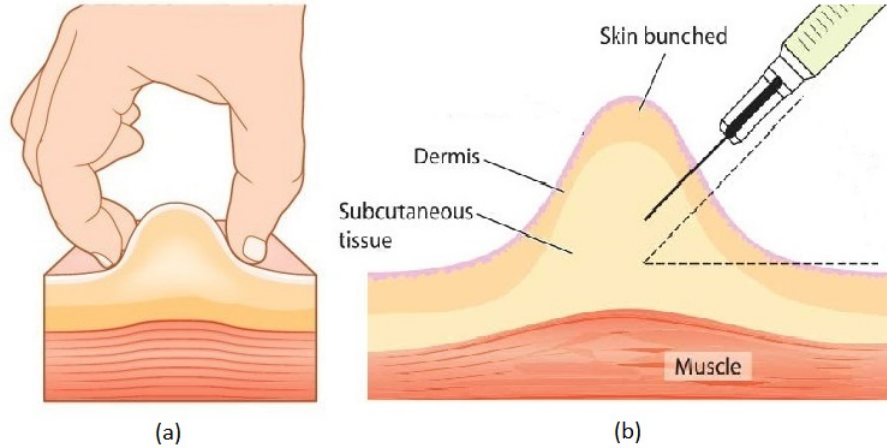


Figure 1: Cartoon diagram of subcutaneous injection (SCI): (a) Skin is bunching during injection, (b) Needle injecting after skin bunched [51].

must be used to avoid the risk of muscle damage. The best method is to lift the skin of the injection site to pull the fat tissue within the SCL away from the underlying ML and hold it for the entire duration of the injection procedure (Fig. 1).

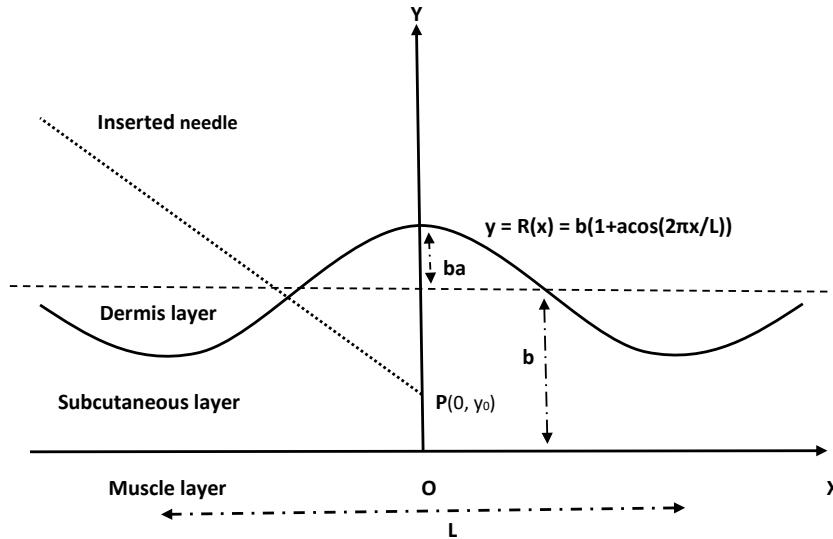


Figure 2: Schematic of the mathematical model approximating the fluid injection process.

Referring to Fig. 2, $(0, y_0)$ is considered as the point of injection, i.e., the position of the tip of the needle. Therefore, $b - y_0$ is the penetration depth from the interface of SCL and DL (may be regarded as SD interface). The SCL is initially bounded by a permeable upper DL (before injection) located at $y = b$ and a permeable lower ML at $y = 0$. If a medical staff takes a big pinch of the patient's skin using the thumb and index fingers and holds,

the SCL gets pulled away from the ML to make the injection easier. Consequently, the interface of SCL and DL (i.e., SD interface) assumes the shape of a cosine curve of the form $y = R(x) = b(1 + a \cos(2\pi x/L))$ within $x \in [-L/2, L/2]$ with a as its amplitude such that ba signifies the increased height of the SCL as a result of skin lifting.

The present study mainly deals with the impact of tissue anisotropy on the motion of injected fluid rather than the time duration of injection. Consequently, one may assume the SCI process described here is time independent. Two major components of the SCL are IF and AC. In general, the cells within SCL are oriented in such a pattern that the overall permeability becomes anisotropic. Subsequently, the SCL can be considered as a deformable porous media or poroelastic media with anisotropic permeability where the cellular phase acts as solid material and the governing equations of biphasic mixture theory can describe the fluid mechanical process within SCL. However, there will be an issue regarding decoupling of one phase from the other in the governing equations under the assumption of steady state [39, 52]. It must be emphasized that the momentum equation for the fluid component does not take into account the solid displacement term. In contrast, the solid constituent's momentum equation does have the fluid velocity term. This may be regarded as a one-way coupling between two principal constituents present within the SCL. In order to avoid such situation, both IF and AC can be assumed to be in the fluid phase with different viscosities [27, 28]. After successful administration of a drug loaded fluid through SC injection, the injected fluid becomes a part of the IF as we consider both of them to have a similar dynamic viscosity. If $\mu_f^{(\text{IF})}$ and $\mu_f^{(\text{D})}$ are the viscosities, $\varphi_f^{(\text{IF})}$ and $\varphi_f^{(\text{D})}$ are the volume fractions of IF and injected drug-loaded fluid respectively, the effective viscosity of IF in presence of injected drug loaded fluid becomes $\mu_f \approx \varphi_f^{(\text{IF})} \mu_f^{(\text{IF})} + \varphi_f^{(\text{D})} \mu_f^{(\text{D})}$. On the other hand, μ_c denotes the viscosity of the adipose cell.

A two-dimensional steady motion of these two incompressible fluids within the SCL is considered. SCL does not allow fast absorption of an injected drug due to the presence of fewer blood vessels Barbieri et al. [53]. Also, within the fat tissue of SCL, the interstitial gap is expected to be small. Consequently, the motions of two incompressible fluid constituents (IF and AC) are governed by Brinkman type equations where the interactions between constituent phases are involved and given by [23, 39]

$$-\varphi_f \nabla P + (\lambda_f + \mu_f) \nabla(\nabla \cdot \mathbf{u}_f) + \mu_f \nabla^2 \mathbf{u}_f - \mu_f \mathbf{K}^{-1}(\mathbf{u}_f - \mathbf{u}_c) = 0, \quad (5)$$

$$-\varphi_c \nabla P + \mu_c \nabla^2 \mathbf{u}_c + \mu_f \mathbf{K}^{-1}(\mathbf{u}_f - \mathbf{u}_c) = 0, \quad (6)$$

In addition, above momentum equations are supported by the following equations of mass conservation:

$$\nabla \cdot (\varphi_f \mathbf{u}_f) = F(x, y), \quad (7)$$

and

$$\nabla \cdot (\varphi_c \mathbf{u}_c) = 0, \quad (8)$$

where $\mathbf{u}_f = (u_f, v_f)$ and $\mathbf{u}_c = (u_c, v_c)$ are the velocity vector for IF and AC respectively; φ_f and φ_c are the volume fraction for IF and AC respectively with $\varphi_f + \varphi_c = 1$; $F(x, y)$

represents the source corresponding to the fluid injection; P is the hydrodynamic pressure. If we drop adipose cell velocity and IF velocity from Eqs. (5) and (6) respectively, we get Brinkman equation (governing momentum equations for flow through a rigid porous media) [45, 54, 55] in each case. Note that the second term on the left-hand side of Eq. (5) arises due to the nonzero source term $F(x, y)$ in the mass conservation equation (7) corresponding to IF. However, in Eq. (6) no such term arises due to the absence of sources in the mass conservation equation (8) for AC since the proliferation of AC is neglected.

Considering the arbitrary orientation of fat and connective tissues within the SCL, the permeability tensor \mathbf{K} possesses both non-zero off-diagonal entries along with dissimilar diagonal elements. In other words, \mathbf{K} may depend on the anisotropic angle ϕ between the horizontal direction and the principal axis [56, 42]. The scenario at hand bears striking similarities to the flow through a porous material that is both deformable and anisotropic. Such materials typically exhibit three distinct sets of directions, including the principal axes of stress and strain, which possess clear and unambiguous physical properties. Detailed anisotropic description of such solid materials can be found in Truesdell and Toupin [16], Truesdell et al. [18]. Our study solely concentrates on a basic scenario where the permeability tensor \mathbf{K} exclusively comprises components that align with the principal directions [44, 45]:

$$\mathbf{K} = \begin{bmatrix} K_1 & 0 \\ 0 & K_2 \end{bmatrix}, \quad (9)$$

with K_1 and K_2 are the permeabilities along the x and y directions (i.e. in principal directions) respectively.

2.1 Boundary conditions:

In order to proceed further and derive the solution of the problem, we consider the following boundary conditions:

(i) At the interface of SCL and DL (SD interface), denoted as $y = R(x)$, the tangential and normal velocity components are assumed as follows:

$$\mathbf{u}_f \cdot \hat{\mathbf{t}} = 0 \quad \text{and} \quad \mathbf{u}_f \cdot \hat{\mathbf{n}} = V_D(x), \quad (10)$$

where $\hat{\mathbf{t}}$ and $\hat{\mathbf{n}}$ are the unit tangent and normal vector respectively on $y = R(x)$. This condition implies that the tangential velocity of IF vanishes at the SD interface, while the normal velocity is equal to the vertical permeation $V_D(x)$ through the interface. On the other hand, at $y = R(x)$, both the velocity components of AC are set to zero:

$$u_c = 0 \quad \text{and} \quad v_c = 0. \quad (11)$$

(ii) At $y = 0$, corresponding to the interface between the SCL and the ML (which may be regarded as the SM interface), the horizontal (tangential) and vertical (normal) velocity

components are assumed to follow as

$$u_f = \lambda_{s_f} \frac{\partial u_f}{\partial y}, \quad v_f = V_M(x), \quad (12)$$

$$u_c = \lambda_{s_c} \frac{\partial u_c}{\partial y} \text{ and } v_c = 0. \quad (13)$$

where λ_{s_f} and λ_{s_c} are the slip coefficients.

The injected fluid (containing drug molecules) dissolved within the interstitial fluid of the SCL can undergo vertical permeation through both the SD and SM interfaces, determined by $V_D(x)$ and $V_M(x)$ respectively. However, it is reasonable to consider that the ACs within the SCL are static on both the SD and SM interfaces so that they cannot permeate through due to their high density and size. These assumptions are reasonable based on the physical characteristics of adipose cells [57]. Therefore, both the SD and SM interfaces act as porous filter which permits IF to undergo a vertical permeation but restricts ACs. An equivalent situation is observed when fluid diffuses through an elastic solid undergoing large deformations [58]. Note that corresponding to the constant flow rate, we can get $V_D(x)$ is equal to $V_M(x)$ (see Theorem 1). The expressions of $V_D(x)$ or $V_M(x)$ are considered later.

The structural difference between the SCL and ML suggests the permeability variation. According to Kim et al. [1] corresponding to the same flow rate in horizontal and vertical directions, the horizontal permeability of the SCL is found to be higher than that of the ML. On the other hand, during the injection procedure, a horizontal motion at the SM interface may be noted due to the variation of fluid pressure (generated from the injection site) in the axial direction. Such motion can be characterized by the boundary conditions Eq. (12)-(13) as proposed by Beavers and Joseph [59], Jones [60], Karmakar and Raja Sekhar [61], and Hill and Straughan [62] at the SM interface are regarded as slip conditions where the parameter λ_s (called slip coefficient) is directly proportional to the length scale same as $\sqrt{K_1}$. In particular, we consider $\lambda_{s_f} = \varphi_f \lambda_s$ and $\lambda_{s_c} = \varphi_c \lambda_s$ (where λ_s is the common slip coefficient at the SD interface).

(iii) Flux condition: Let Q be the volumetric flow rate across the region which is given by

$$Q = \int_0^{R(x)} (\varphi_f u_f + \varphi_c u_c) dy. \quad (14)$$

2.2 Non-dimensionalisation

We introduce the following non-dimensional variables:

$x' = x/L$, $y' = y/b$, $\delta = b/L$, $u'_i = u_i/(Q/b)$, $v'_i = v_i/(Q/L)$, $p' = p/(\mu_f QL/K_1 b)$, for $i = f, c$ in Eqs. (5)-(8) to make them dimensionless. Accordingly, we obtain following dimensionless parameters those appear in the dimensionless governing equations: $\mu_r = \mu_f/\mu_c$, $Da = K_1/b^2$, $\lambda^2 = K_1/K_2$, $V'_D = V_D/(Q/L)$, $V'_M = V_M/(Q/L)$, $\lambda'_s = \lambda_s/L$ and $F' = F/(Q/bL)$.

Here, δ denotes the aspect ratio of the SCL; Da is the ease of interstitial fluid percolation through the SC tissue in the horizontal direction (equivalent to the Darcy number); μ_r is the ratio of the IF to the AC and λ^2 is the ratio of horizontal permeability to the vertical permeability, which can be referred to as the anisotropic ratio.

Correspondingly, the non-dimensional governing equations can be written as (omitting dash)

$$\delta^2 \left(1 + \frac{\lambda_f}{\mu_f}\right) \frac{\partial}{\partial x} \left(\frac{\partial u_f}{\partial x} + \frac{\partial v_f}{\partial y}\right) + \left(\delta^2 \frac{\partial^2 u_f}{\partial x^2} + \frac{\partial^2 u_f}{\partial y^2}\right) - \alpha^2 \left[(u_f - u_c) + \varphi_f \frac{\partial p}{\partial x}\right] = 0, \quad (15)$$

$$\delta^2 \left(1 + \frac{\lambda_f}{\mu_f}\right) \frac{\partial}{\partial y} \left(\frac{\partial u_f}{\partial x} + \frac{\partial v_f}{\partial y}\right) + \delta^2 \left(\delta^2 \frac{\partial^2 v_f}{\partial x^2} + \frac{\partial^2 v_f}{\partial y^2}\right) - \alpha^2 \left[\delta^2 \lambda^2 \alpha^2 (v_f - v_c) + \varphi_f \frac{\partial p}{\partial y}\right] = 0, \quad (16)$$

$$\left(\delta^2 \frac{\partial^2 u_c}{\partial x^2} + \frac{\partial^2 u_c}{\partial y^2}\right) + \left[\alpha^2 \mu_r (u_f - u_c) - \varphi_c \frac{\partial p}{\partial x}\right] = 0, \quad (17)$$

$$\delta^2 \left(\delta^2 \frac{\partial^2 v_c}{\partial x^2} + \frac{\partial^2 v_c}{\partial y^2}\right) + \alpha^2 \mu_r \left[\delta^2 \lambda^2 (v_f - v_c) - \varphi_c \frac{\partial p}{\partial y}\right] = 0, \quad (18)$$

$$\left(\frac{\partial u_f}{\partial x} + \frac{\partial v_f}{\partial y}\right) = F(x, y), \quad (19)$$

$$\left(\frac{\partial u_c}{\partial x} + \frac{\partial v_c}{\partial y}\right) = 0, \quad (20)$$

where $\alpha^2 = 1/Da$. Here we consider Stokes hypothesis by taking $2\lambda_f + 3\mu_f = 0$, i.e. $\lambda_f/\mu_f = -3/2$ [39]. Also the corresponding boundary conditions are (dropping dash)

(i) on $y = R(x) = 1 + a \cos(2\pi x)$,

$$u_f = 2\pi a \delta^2 \frac{\sin(2\pi x)}{\sqrt{1 + 4\pi^2 a^2 \delta^2 \sin(2\pi x)}} V_D(x), \quad v_f = \frac{1}{\sqrt{1 + 4\pi^2 a^2 \delta^2 \sin(2\pi x)}} V_D(x), \quad (21)$$

$$u_c = 0 \quad \text{and} \quad v_c = 0. \quad (22)$$

(ii) on $y = 0$,

$$u_f = \varphi_f \lambda_s \frac{\partial u_f}{\partial y}, \quad v_f = V_M(x), \quad (23)$$

$$u_c = \varphi_c \lambda_s \frac{\partial u_c}{\partial y} \quad \text{and} \quad v_c = 0. \quad (24)$$

(iii) Flux condition: The non-dimensional volumetric flow rate is given by

$$1 = \int_0^{R(x)} (\varphi_f u_f + \varphi_c u_c) dy. \quad (25)$$

3 Perturbation approximation

In order to solve the above boundary value problem, we can use the perturbation method to find an approximate solution [63, 38, 45]. We assume that the aspect ratio (δ) of the region is small, i.e. $\delta^2 \ll 1$, and this allows us to apply perturbation theory. Accordingly, with respect to the small parameter δ^2 , we can expand the velocity and pressure in a perturbation series as:

$$(u_i, v_i, p) = (u_{i_0}, v_{i_0}, p_0) + \delta^2(u_{i_1}, v_{i_1}, p_1) + O(\delta^4), \quad \text{for } i = f, c. \quad (26)$$

The first order correction is δ^2 , since no terms of order δ appear in the governing equations and boundary conditions. The flow field is solved by collecting the similar powers of δ^2 .

3.1 The leading-order problem

The governing equations reduce to

$$\frac{\partial^2 u_{f_0}}{\partial y^2} - \alpha^2 \left[(u_{f_0} - u_{c_0}) + \varphi_f \frac{\partial p_0}{\partial x} \right] = 0, \quad (27)$$

$$\frac{\partial^2 u_{c_0}}{\partial y^2} + \alpha^2 \mu_r \left[(u_{f_0} - u_{c_0}) - \varphi_c \frac{\partial p_0}{\partial x} \right] = 0, \quad (28)$$

$$\frac{\partial p_0}{\partial y} = 0, \quad (29)$$

$$\left(\frac{\partial u_{f_0}}{\partial x} + \frac{\partial v_{f_0}}{\partial y} \right) = F(x, y), \quad (30)$$

$$\left(\frac{\partial u_{c_0}}{\partial x} + \frac{\partial v_{c_0}}{\partial y} \right) = 0. \quad (31)$$

The corresponding boundary conditions are

(i) on $y = R(x)$,

$$u_{f_0} = 0, v_{f_0} = V_D(x), \quad (32)$$

$$u_{c_0} = 0 \text{ and } v_{c_0} = 0. \quad (33)$$

(ii) on $y = 0$

$$u_{f_0} = \lambda_s \frac{\partial u_{f_0}}{\partial y}, v_{f_0} = V_M(x), \quad (34)$$

$$u_{c_0} = \lambda_s \frac{\partial u_{c_0}}{\partial y} \text{ and } v_{c_0} = 0. \quad (35)$$

(iii) Flux condition

$$1 = \int_0^{R(x)} (\varphi_f u_{f_0} + \varphi_c u_{c_0}) dy. \quad (36)$$

Theorem 1. *The vertical permeation velocities $V_D(x)$ and $V_M(x)$ are equal when*

$$1 = \int_0^{R(x)} (\varphi_f u_f + \varphi_c u_c) dy$$

Proof. If we differentiate

$$\int_0^{R(x)} (\varphi_f u_{f_0} + \varphi_c u_{c_0}) dy = 1,$$

under the integration sign using Leibnitz rule, we obtain

$$(\varphi_f u_{f_0} + \varphi_c u_{c_0})(x, R(x)) \frac{dR(x)}{dx} + \int_0^{R(x)} \left(\varphi_f \frac{\partial u_{f_0}}{\partial x} + \varphi_c \frac{\partial u_{c_0}}{\partial x} \right) dy = 0,$$

which implies

$$(\varphi_f u_{f_0}(x, R(x)) + \varphi_c u_{c_0}(x, R(x))) \frac{dR(x)}{dx} + \int_0^{R(x)} \left(\varphi_f \left(-\frac{\partial v_{f_0}}{\partial y} \right) + \varphi_c \left(-\frac{\partial v_{c_0}}{\partial y} \right) \right) dy = 0.$$

After some simplification,

$$(\varphi_f v_{f_0} + \varphi_c v_{c_0})(y = R(x)) - (\varphi_f v_{f_0} + \varphi_c v_{c_0})(y = 0) = 0.$$

Hence,

$$V_D(x) = V_M(x).$$

□

3.2 The $O(\delta^2)$ problem

The governing equations corresponding to the first order are

$$-\varphi_f \alpha^2 \frac{\partial p_1}{\partial x} + \left(1 + \frac{\lambda_f}{\mu_f} \right) \frac{\partial}{\partial x} \left(\frac{\partial u_{f_0}}{\partial x} + \frac{\partial v_{f_0}}{\partial y} \right) + \left(\frac{\partial^2 u_{f_0}}{\partial x^2} + \frac{\partial^2 u_{f_1}}{\partial y^2} \right) - \alpha^2 (u_{f_1} - u_{c_1}) = 0, \quad (37)$$

$$-\varphi_f \alpha^2 \frac{\partial p_1}{\partial y} + \left(1 + \frac{\lambda_f}{\mu_f} \right) \frac{\partial}{\partial y} \left(\frac{\partial u_{f_0}}{\partial x} + \frac{\partial v_{f_0}}{\partial y} \right) + \frac{\partial^2 v_{f_0}}{\partial y^2} - \alpha^2 \lambda^2 (v_{f_0} - v_{c_0}) = 0, \quad (38)$$

$$-\varphi_c \mu_r \alpha^2 \frac{\partial p_1}{\partial x} + \left(\frac{\partial^2 u_{c_0}}{\partial x^2} + \frac{\partial^2 u_{c_1}}{\partial y^2} \right) + \mu_r \alpha^2 (u_{f_1} - u_{c_1}) = 0, \quad (39)$$

$$-\varphi_c \mu_r \alpha^2 \frac{\partial p_1}{\partial y} + \frac{\partial^2 v_{c_0}}{\partial y^2} + \mu_r \alpha^2 \lambda^2 (v_{f_0} - v_{c_0}) = 0, \quad (40)$$

$$\varphi_f \left(\frac{\partial u_{f_1}}{\partial x} + \frac{\partial v_{f_1}}{\partial y} \right) = 0, \quad (41)$$

$$\varphi_c \left(\frac{\partial u_{c_1}}{\partial x} + \frac{\partial v_{c_1}}{\partial y} \right) = 0. \quad (42)$$

Corresponding boundary conditions reduce to

(i) on $y = R(x)$,

$$u_{f_1} = 2\pi a^2 \sin(2\pi x) V_D(x), \quad v_{f_1} = -2\pi^2 a^2 \sin(2\pi x) V_D(x), \quad (43)$$

$$u_{c_1} = 0 \text{ and } v_{c_1} = 0. \quad (44)$$

(ii) on $y = 0$,

$$u_{f_1} = \lambda_s \frac{\partial u_{f_1}}{\partial y}, \quad v_{f_1} = 0, \quad (45)$$

$$u_{c_1} = \lambda_s \frac{\partial u_{c_1}}{\partial y} \text{ and } v_{c_1} = 0. \quad (46)$$

(iii) Flux condition

$$0 = \int_0^{R(x)} (\varphi_f u_{f_1} + \varphi_c u_{c_1}) dy. \quad (47)$$

3.3 Structure of the source term $F(x, y)$

In Eq. (30), $F(x, y)$ represents the tip of the needle of the syringe at some point inside the SCL. One can think of a point source at the point $(0, y_0)$ (see Fig. 2) which can be expressed as

$$F(x, y) = m_0 \delta(x) \delta(y - y_0), \quad (48)$$

where m_0 represents the strength of the point source. One can solve the leading order and first order equations using finite difference scheme by discretizing the domain while keeping the point $(0, y_0)$ outside the meshgrid. However, one can attempt for the analytical solution in the regions $y < y_0$ and $y > y_0$ for all values of x . Since $y = y_0$ is a line on which injection point (tip of needle) must lie, thus the following conditions at $y = y_0$ can be used to match the solution :

$$u_{f_0}(x, y_0^+) = u_{f_0}(x, y_0^-),$$

$$u_{c_0}(x, y_0^+) = u_{c_0}(x, y_0^-),$$

and

$$\frac{\partial u_{f_0}(x, y)}{\partial y} \Big|_{y=y_0^+} = \frac{\partial u_{f_0}(x, y)}{\partial y} \Big|_{y=y_0^-},$$

$$\frac{\partial u_{c_0}(x, y)}{\partial y} \Big|_{y=y_0^+} = \frac{\partial u_{c_0}(x, y)}{\partial y} \Big|_{y=y_0^-}.$$

3.4 Subcutaneous tissue velocity and stream function

We define subcutaneous tissue velocity or composite velocity $\mathbf{u} = (u, v)$ of the mixture of IF and AC presents in the SCL as

$$\mathbf{u} = \varphi_f \mathbf{u}_f + \varphi_c \mathbf{u}_c \quad (49)$$

If Φ_f and Φ_c are the stream function of the IF and AC respectively that are present in the SCL, then their relation with the velocity components are

$$u_f = \frac{\partial \Phi_f}{\partial y}, u_c = \frac{\partial \Phi_c}{\partial y} \text{ and } v_f = -\frac{\partial \Phi_f}{\partial x}, v_c = -\frac{\partial \Phi_c}{\partial x}.$$

Also, we define the composite stream function of the mixture as

$$\Phi = \varphi_f \Phi_f + \varphi_c \Phi_c \quad (50)$$

In the SCL, the quantity of IF is much larger than the quantity of AC. Thus the subcutaneous tissue velocity or composite velocity and stream function can be considered in macroscopic level [34, 32]. The spreading of the injected fluid within the interstitial space of the subcutaneous tissue can be manifested by the streamline pattern exhibited by the composite motion of IF and AC.

Theorem 2. *If $\Phi_i (i = f, c)$ are the stream functions defined as*

$$\Phi_i = \begin{cases} \Phi_i^{(1)}, & 0 \leq y < y_0 \\ \Phi_i^{(2)}, & y_0 < y \leq R(x) \end{cases}$$

and there exists ψ_i satisfying $\psi_i = \int u_i dy$ such that

$$\psi_i = \begin{cases} \psi_i^{(1)}, & 0 \leq y < y_0 \\ \psi_i^{(2)}, & y_0 < y \leq R(x), \end{cases}$$

then the following relations hold

$$\Phi_i^{(1)}(x, y) = \psi_i^{(1)}(x, y) + f_i(x),$$

$$\Phi_i^{(2)}(x, y) = \psi_i^{(2)}(x, y) + g_i(x),$$

for arbitrary function $f_i(x)$ and $g_i(x)$.

Proof. The stream function is related to the velocity components by the relations

$$u_i = \frac{\partial \Phi_i}{\partial y} \text{ and } v_i = -\frac{\partial \Phi_i}{\partial x}.$$

Considering the first relation

$$u_i = \frac{\partial \Phi_i}{\partial y},$$

or

$$\Phi_i = \int u_i dy + h(x),$$

where $h(x)$ is obtained from the integration. Let $\psi_i(x, y) = \int u_i dy$.

Since u_i and v_i are defined in two regions (say $u_i^{(1)}$, $u_i^{(2)}$ and $v_i^{(1)}$, $v_i^{(2)}$), thus we have stream function in the regions as

$$\Phi_i^{(1)}(x, y) = \psi_i^{(1)}(x, y) + f_i(x), \quad \text{if } 0 \leq y < y_0$$

$$\Phi_i^{(2)}(x, y) = \psi_i^{(2)}(x, y) + g_i(x). \quad \text{if } y_0 \leq y < R(x)$$

Next we have to find the functions $f_i(x)$ and $g_i(x)$.

Since stream function is continuous, thus we have

$$\Phi_i^{(1)}(x, y_0^-) = \Phi_i^{(2)}(x, y_0^+),$$

which gives

$$f_i(x) = \psi_i^{(2)}(x, y) - \psi_i^{(1)}(x, y) + g_i(x).$$

Also since

$$\Phi_i^{(2)}(x, y) = \psi_i^{(2)}(x, y) + g_i(x),$$

Upon taking derivative on both sides with respect to x , we have

$$\frac{\partial \Phi_i^{(2)}}{\partial x} = \frac{\partial \psi_i^{(2)}}{\partial x} + g_i'(x),$$

which gives

$$g_i'(x) = -\frac{\partial \psi_i^{(2)}}{\partial x} - v_i^{(2)}(x, y).$$

Now integrating both sides, we get

$$g_i(x) = -\psi_2(x, y) - \int v_i^{(2)}(x, y) dx,$$

which satisfies throughout the considered region.

Thus at $y = R(x)$,

$$g_i(x) = -\psi_2(x, R(x)) - \int v_i^{(2)}(x, R(x)) dx.$$

Since $v_i^{(2)}(x, R(x))$ is a known function (which we obtain using boundary conditions), thus we get $g_i(x)$ and using this we can obtain $f_i(x)$ easily from the continuity condition of stream function. \square

The detailed solution of the leading order and $O(\delta^2)$ problem corresponding to IF and AC are shown in Appendix A and Appendix B respectively.

4 Results and Discussion

In this study, a flow-induced by fluid injection has been considered within the anisotropic SCL which is bounded by permeable DL from the topside and permeable ML from the bottom. As per the present mathematical model is concerned, the principal components of the SCL are AC (fat tissue) and IF with a large proportion of fluid part. Consequently, φ_f is chosen within the range $0.7 \leq \varphi_f \leq 0.9$ throughout the study (see Khor et al. [64], Truskey et al. [65]). All the flow parameters such as λ , μ_r , δ , a , Da , λ_s are reported in Table 1 with their reference ranges and are chosen based on experimental or theoretical studies already existed in literature. The analysis underlying the consideration of parameter ranges is discussed below. For example, (Da) which is the ease of fluid percolation in the horizontal direction can be considered within the range $10^{-3} \leq Da \leq 5 \times 10^{-3}$ following Dey and Raja Sekhar [39]. Based on the choice of Da , we specify the slip coefficient λ_s within the range $0.001 \leq \lambda_s \leq 0.05$ as the value of it is up to $O(\sqrt{Da})$. Note that $\lambda_s \rightarrow 0$ makes

Parameter	Range	Remark
Anisotropic ratio (λ)	$0.5 < \lambda \leq 2$	Shrestha and Stoeber [13]
Viscosity ratio (μ_r)	$0 < \mu_r < 1$	Considered
Da	$10^{-3} \leq Da \leq 5 \times 10^{-3}$	Dey and Raja Sekhar [39]
Amplitude of the wavy layer (a)	$0.34 \leq a \leq 0.5$	Considered
Aspect ratio of the region (δ)	$0.1 \leq \delta \leq 0.3$	Karmakar and Raja Sekhar [45]
Slip coefficient (λ_s)	$0.001 \leq \lambda_s \leq 0.05$	Dey and Raja Sekhar [39]

Table 1: Various parameters involved in this study with their range.

the adipose cellular phase rigid towards the squeezing effect at the SM interface due to the fluid pressure at the line of injection. On the other hand, the choice of λ is prompted by the study of Shrestha and Stoeber [13] which reports the optimum value of permeability of skin tissue lies within the range $0.59 \times 10^{-14} \text{ m}^2$ to $2.10 \times 10^{-12} \text{ m}^2$. Therefore, one can consider K_1 and K_2 lying between the above range. Consequently, λ lies within the range $0.53 \leq \lambda \leq 2$. Except for $\lambda = 1$ (isotropic), anisotropic behavior is exhibited for all values of λ within the above range. The perturbation parameter δ is the ratio between the SCL depth and the SCL length trapped inside the thumb and pointer of the medical staff during the injection. Essentially, we have $\delta^2 \ll 1$ for this study. A similar parameter has been observed in the study of Karmakar and Raja Sekhar [45] and consequently, we opt the magnitude of δ within the range $0.1 \leq \delta \leq 0.3$. A sensitivity analysis associated with the choosing δ with the help of λ is shown in Table 2. In general, the adipose cellular phase should have a higher viscosity compared to the interstitial fluid (IF) within the same continuum description. This is because adipose cells, or adipocytes, are lipid-rich cells with a lipid viscosity of 36.8 mPa.s

or $36.8 \times 10^{-3} \text{ kgm}^{-1}\text{s}^{-1}$ [66], while the viscosity of the interstitial fluid can be approximated as $3.5 \times 10^{-3} \text{ kgm}^{-1}\text{s}^{-1}$ by following the study of Yao et al. [67]. Hence, the viscosity ratio $\mu_r = \mu_f/\mu_c$ can be chosen to lie within the range $0 < \mu_r < 1$.

$V_M(x)$ represents the permeation velocity at the SM interface which can be expressed as

λ	$\delta^2(\ll 1)$	$\delta^2\lambda^2(\ll 1)$
1	0.09	0.09
1.5	0.09	0.2025
1.75	0.09	0.2756
2	0.09	0.36

Table 2: Various tissue anisotropic ratio (λ) magnitude, aspect ratio (δ) value and corresponding value of $\delta^2\lambda^2$.

follows

$$V_M(x) = V_{M_0} + \sigma_M \left(\frac{dp_0}{dx} \right), \quad (51)$$

where V_{M_0} is the permeation velocity at constant leading order pressure. Note that Eq. (51) is analogous to Darcy law defined at the SM interface. Understanding the impact of the coefficient σ_M on permeation regulation is absolutely crucial, particularly in the presence of varying pressure. It should be noted that $V_M(x)$ is directly linked to the gradient of the leading order pressure, as it represents the vertical component of the interfacial velocity at $y = 0$. Evidently, the minimum value of $V_M(x)$ is V_{M_0} , assuming a positive pressure gradient near the SM interface. In order to determine the minimum value of $V_M(x)$, it is imperative that we ensure dp_0/dx is equal to zero on SM interface (please refer Fig. 2). At the point $(x, y) = (0, 0)$ on the SM interface, the skin pinching depth attains its maximum as per the schematic in Fig. 2. Some algebra on dp_0/dx obtains

$$\frac{dp_0}{dx} = \frac{\alpha^2}{4} \mu_r (1 + \mu_r) \left(a - \frac{1}{3} \right), \quad \text{at } x = 0. \quad (52)$$

Clearly, $(dp_0/dx)_{x=0} \geq 0$ as $a \geq 1/3$. Hence, $V_M(x=0)$ is the permeation velocity at $x = 0$ from SCL to ML. Permeation velocity can also be achieved at other points $x = x_0$ on the SM interface, where x_0 is not equal to zero. σ_M , as per Eq. (51), represents the difference in permeation velocity at $x = o$ and the lowest possible permeation velocity per unit gradient of pressure calculated at $x = 0$ on the SM interface. Therefore, from Eqs. (51)-(52) it follows

$$\frac{V_M(0) - V_{M_0}}{\sigma_M} = \frac{\alpha^2}{4} \mu_r (1 + \mu_r) \left(a - \frac{1}{3} \right), \quad (53)$$

which says $V_M(0)$ is equal to V_{M_0} when the value of a is equal to $1/3$. This means that more than one-third of the SCL depth needs to be pinched up. Eventually, Table 3 indicates that the maximum depth of SCL produced for injection varies depending on the type of skin lifting. Fig. 3 demonstrates a noticeable increase in the difference between $V_M(0)$ and V_{M_0}

as the value of μ_r increases for various pinching depths between $a = 0.35$ and $a = 0.4$. This suggests that the permeation velocity increases with the pinching depth and μ_r . To achieve optimal permeation, increasing the skin pinching depth beyond $a = 1/3$ is recommended. Similar analysis as above can be done at other locations of SM interface. Additionally, using highly viscous fluid may enhance permeation, although the negative effects of high viscosity must be considered. Further discussion on this topic can be found in the study later.

In order to understand the flow pattern of injected fluid within the SCL, we compute the

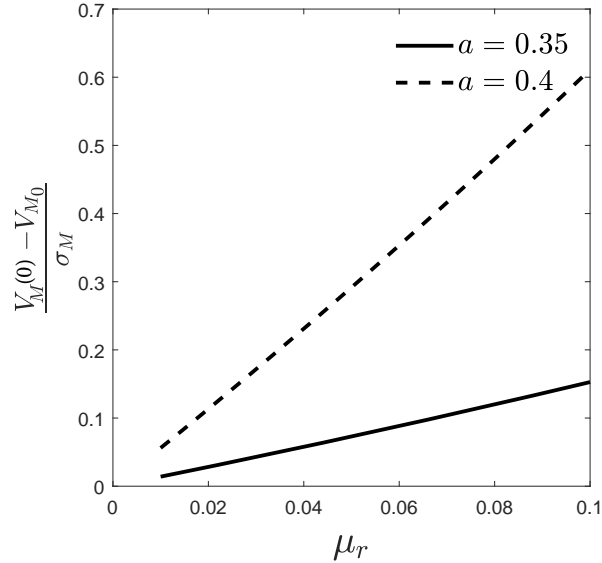


Figure 3: Variation of $(V_M(0) - V_{M_0}) / \sigma_M$ with respect to μ_r when $a = 0.35$ and $a = 0.4$ corresponding to $Da = 3 \times 10^{-3}$.

Nature of skin lifting	Maximum depth of the SCL for injection
Higher pinching depth ($a = 0.45$)	$R(0) = 1.45$
Moderate pinching depth ($a = 0.4$)	$R(0) = 1.4$
Minimum required pinching depth ($a = 0.34$)	$R(0) = 1.34$

Table 3: Various types of skin lifting and the corresponding height of the skin produced for Subcutaneous injection

streamlines corresponding to the composite velocity. The corresponding flow patterns are recognized and explored using three important parameters a , μ_r and λ . The behavior of the flow patterns are discussed using axial composite velocity as a function of y and computed shear stress at three positions of y : (i) line of injection ($y = y_0$) (ii) SM interface ($y = 0$) and (iii) SD interface ($y = R(x)$). In the upcoming sections, we are going to discuss this in detail.

4.1 Flow pattern of the injected fluid in terms of Composite Streamlines

The injection fluid's flow patterns containing the drug are illustrated in Figs. 4(a)-4(b) which display composite streamlines (Φ) for two different values of $a = 0.34$ and $a = 0.4$ respectively. The remaining parameters assume the following values: $Da = 3 \times 10^{-3}$, $\delta = 0.3$, $\lambda = 2$, $\mu_r = 0.01$, $\lambda_s = 0.05$. The development of closed contours is observed from the line of injection in the form of primary eddy due to the evolution of high pressure. In addition, the streamlines follow the curvature of the SCL and generate additional closed contours as secondary eddy structures within the lifted portion of the SCL. The secondary eddy structure becomes more pronounced with higher pinching depth a . If we locate a particular contour, say $c = 0.8$, formed near the line of injection, the corresponding size increases with a . This phenomenon is due to the constant transfer of kinetic energy (KE) from a large to a small eddy until the dissipation of KE. The formation of eddies helps better mixing of drug loaded injected fluid with the IF than pure molecular diffusion. In other words, a higher pinching depth causes better assimilation of the injected fluid with the IF.

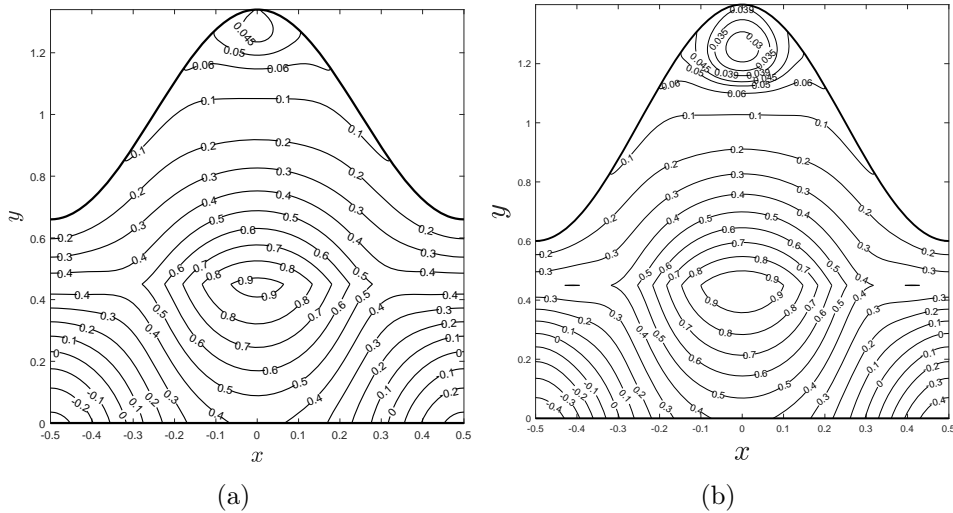


Figure 4: Composite streamlines within the subcutaneous layer for two different pinching depths (a) $a = 0.34$, (b) $a = 0.4$ with other parameters are $\lambda = 2$, $Da = 3 \times 10^{-3}$, $\delta = 0.3$, $\mu_r = 0.01$ and $\lambda_s = 0.05$, when $y_0 = 0.45$ is the line of injection.

The variations in the flow pattern of the injected fluid inside SCL are explained in terms of Φ and depicted through Figs. 5(a)-5(d) for a wide variety of tissue anisotropy (λ). Among all considered values of λ , Fig. 5(a) corresponds to the isotropic nature of the SCL, and the rest are plotted for anisotropic nature, in particular when the horizontal permeability K_1 is greater than the vertical permeability K_2 . When Da is fixed, an increase in λ results in a reduction of the tissue anisotropy along the vertical direction. Consequently, the streamlines in the upstream follow the shape of the SD interface where the skin is pinched up until

$\lambda \approx 1.5$ (see Fig. 5(a)). After that, the flow in the upstream starts to digress following the shape of the interface (see Fig. 5(b)). Corresponding to $\lambda = 1.75$ and 2 onset of the secondary eddy structure causing flow circulation can be seen at the position where the skin is lifted (see Figs. 5(c) and 5(d)). As discussed in the previous paragraph, the secondary eddy structure aftermaths good mixing of injected fluid with the IF. Hence, the movement of the injected drug within the SC tissue region becomes vigorous in case of larger tissue anisotropy and high lifting of the skin.

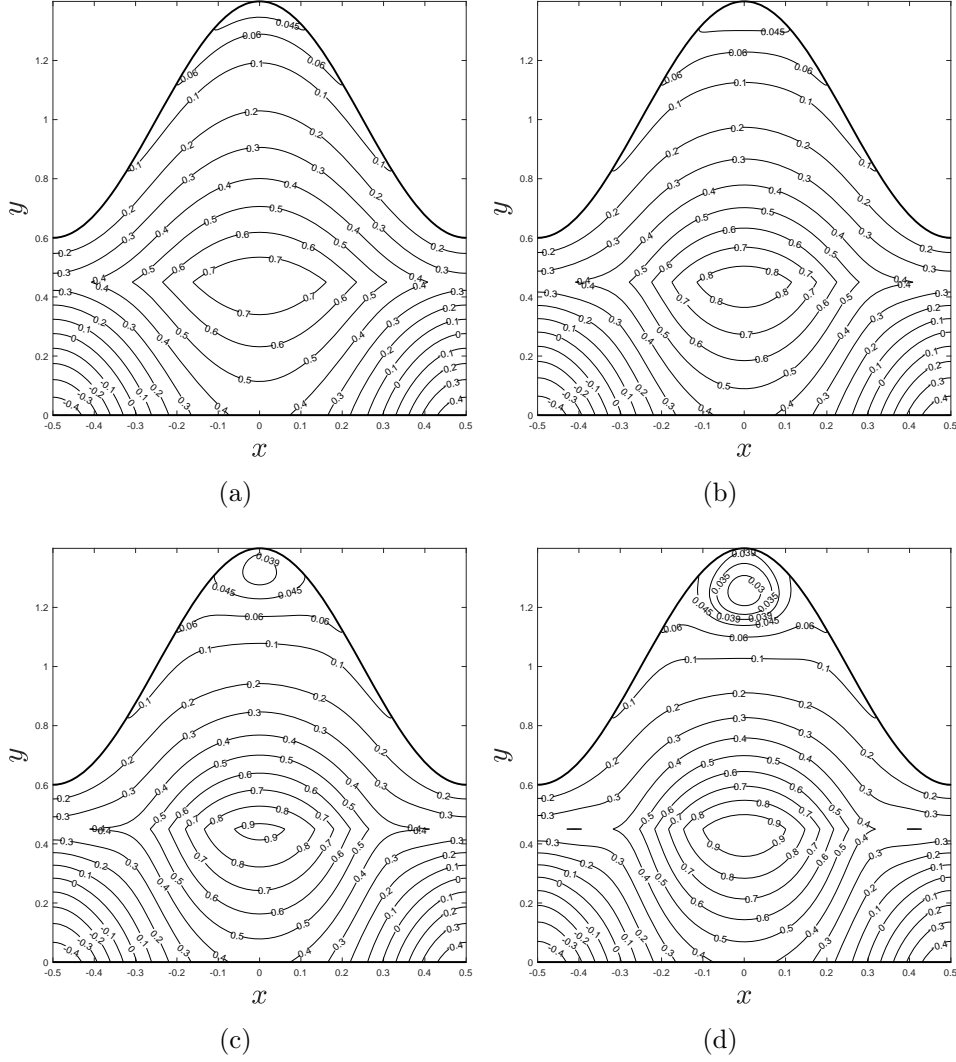


Figure 5: Composite streamlines within subcutaneous layer for different tissue anisotropy ratio (a) $\lambda = 1$, (b) $\lambda = 1.5$, (c) $\lambda = 1.75$ and (d) $\lambda = 2$ with $a = 0.4$, $Da = 3 \times 10^{-3}$, $\delta = 0.3$, $\mu_r = 0.01$ and $\lambda_s = 0.05$, when $y_0 = 0.45$ is the line of injection.

In general, the IF is less viscous than that of the AC population. Consequently, μ_r is less than 1 (i.e., $\mu_f < \mu_c$). So, the AC phase experiences less drag from the IF side. In other words, the

AC can impose high interstitial resistance towards IF movement during fluid injection. Figs. 6(a)-6(c) illustrate the flow pattern of the injected fluid for $\mu_r = 0.1$, $\mu_r = 0.05$ and $\mu_r = 0.01$. Only primary eddies are developed near the SD interface for $\mu_r = 0.1$. But corresponding to the reduced μ_r , a significant viscosity difference between AC and IF is developed. The development of secondary eddy can be observed at the lifted portion for $\mu_r = 0.05$, which becomes prominent with a further decrement of μ_r . We can locate a contour $c = 0.7$ when the viscosity ratio is as low as $\mu_r = 0.1$ close to the line of injection, which subsequently increases in size for smaller μ_r (Fig. 6(b)). Hence $\lambda \geq 1.75$, $a \geq 0.4$, and $\mu_r \leq 0.01$ are the conditions to be satisfied simultaneously to support eddy structure within the lifted portion of the skin.

4.2 Flow pattern of the injected fluid in terms of Composite Velocity

In order to justify the behavior of the composite streamlines, we go through the axial composite velocity (u) profiles as shown in Figs. 7(a)-7(c) for the above three parameters a , λ and μ_r . We identify three intervals for y such as (i) $0 < y \leq 0.4$ (ii) $0.4 < y \leq 1$ (iii) $1 \leq y \leq 1.4$ in which u shows varied behavior due to the assumption of constant volumetric flux condition. This phenomenon justifies the dissipation of a particular contour within the primary eddy after getting larger (with an increase in a) and simultaneously creating new smaller contours within the secondary eddy. Consequently, an increased magnitude of the axial composite velocity with a is noted for ranges of y in (i) and (iii), indicating the role of enhanced axial convective transport corresponding to deeper skin pinching (see Fig. 7(a)). On the other hand, within the range $0.4 < y \leq 1$, u shows change in sign for both $a = 0.34$ and $a = 0.4$ indicating the formation of the secondary eddy.

The influence of tissue anisotropy on generating secondary eddy can be discussed using the axial composite velocity u . Fig. 7(b) represents profiles of u versus y at $x = 0$ for various λ when $a = 0.4$, $\mu_r = 0.01$, $\lambda_s = 0.05$, $Da = 3 \times 10^{-3}$, and $\delta = 0.3$. At the SD interface, u becomes zero due to the no-slip condition, while the IF and AC exhibit horizontal motion at the SM interface due to the slip velocity associated with the squeezing effect under high pressure developed due to SC injection. Except in the interval $0.4 \leq y \leq 1$, u increases with λ while an opposite behavior is noted within the stated region. Such contrasting behavior of u is due to the fixed volumetric flow rate across the SC region. Moreover, u does not change its sign for $\lambda = 1, 1.5$. Still, it changes from positive to negative for $\lambda = 1.75, 2$ indicating the development of a secondary eddy structure near the SD interface where the skin is lifted.

Finally, Fig. 7(c) shows that the composite velocity near the SD and SM interface is decreased with an increasing magnitude of μ_r . However, the opposite phenomenon is noticed near the line of injection. Also, axial composite velocity changes its sign for $\mu_r = 0.01$ while it does not change for $\mu_r = 0.05$ and $\mu_r = 0.1$ which becomes the root cause of prominent secondary eddy structure corresponding to $\mu_r = 0.01$. The development of two eddies may be discussed with the help of pressure gradient and shear stress at the three positions of y , i.e., $y = 0$,

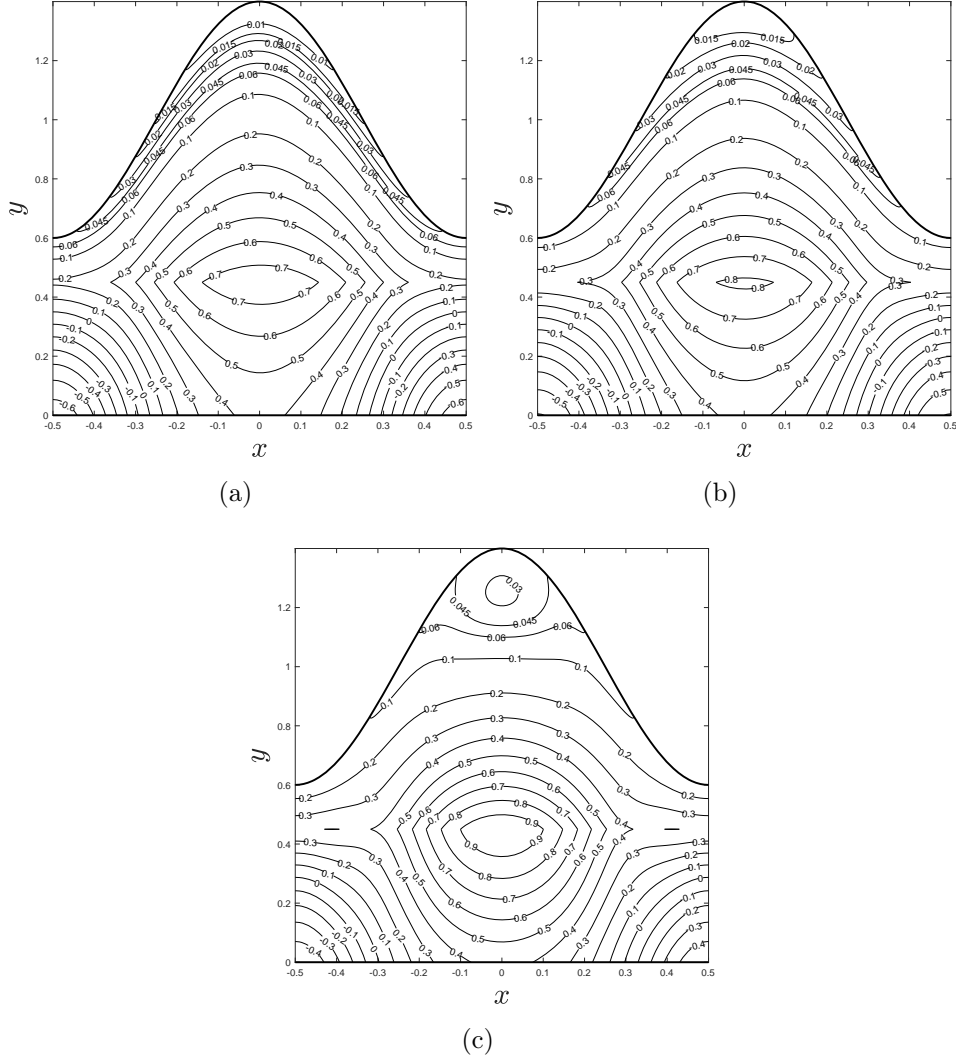


Figure 6: Patterns of composite streamlines within subcutaneous layer for different viscosity ratio (a) $\mu_r = 0.1$, (b) $\mu_r = 0.05$ and (c) $\mu_r = 0.01$ with the other parameters are $\lambda = 2$, $Da = 3 \times 10^{-3}$, $\delta = 0.3$, $a = 0.4$ and $\lambda_s = 0.05$, when $y = y_0 (= 0.45)$ is the line of injection.

$y = y_0$, and $y = R(x)$.

4.3 Effect of pressure gradient and shear stress on pain realization

During and post-injection, a patient may realize swelling and pain from the injection site. According to some researchers, both the pressure gradient and shear stress act as an indicator of the evolvement of physical pain [68, 69]. Consequently, it is necessary to explore the nature of the pressure gradient ($\partial p / \partial x$) and shear stress mainly at three different positions $y = y_0$ (line of injection), $y = 0$ (SM interface) and $y = R(x)$ (SD interface). Figs. 8(a)-8(c) illustrate that the pressure gradient within $[-0.5, 0.5]$ becomes symmetric about the line

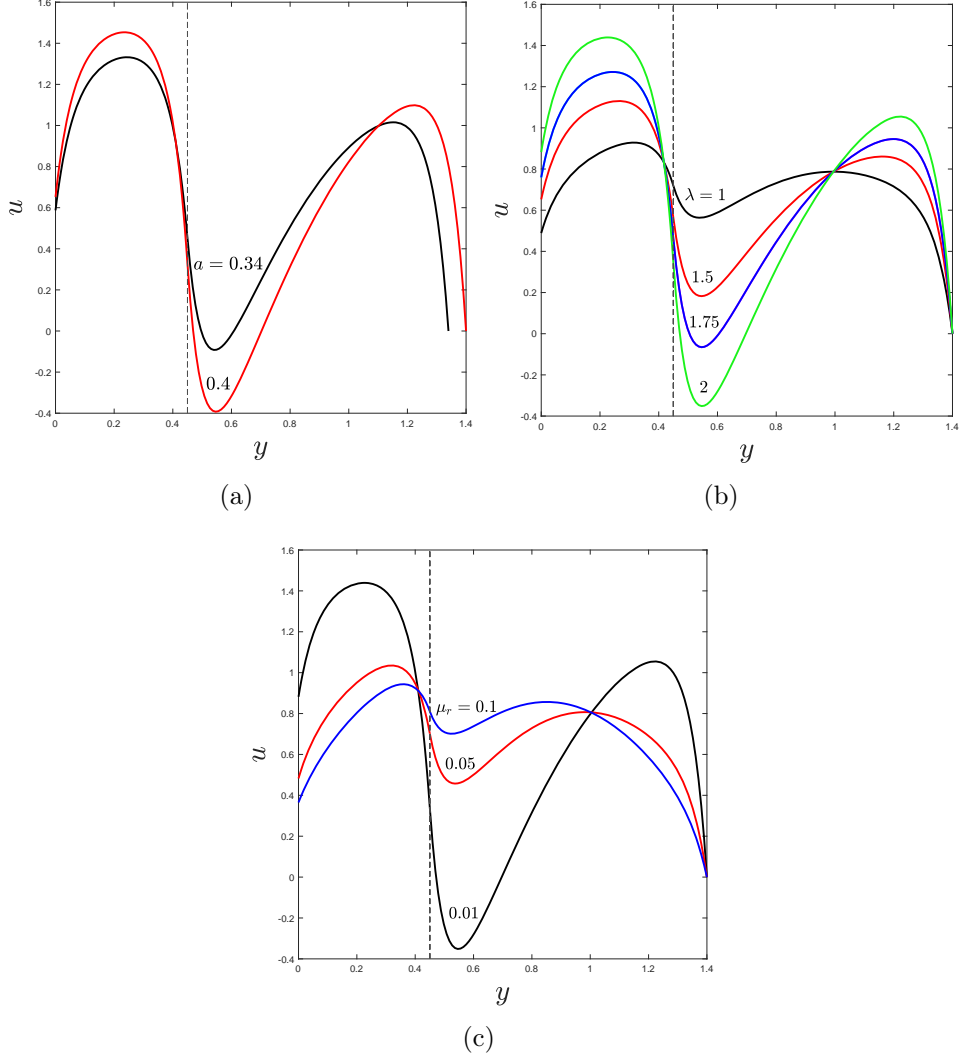


Figure 7: Axial composite velocity versus y for (a) $a = 0.34, 0.4$, (b) $\lambda = 1, 1.5, 1.75, 2$ and (c) $\mu_r = 0.01, 0.05, 0.1$ at $x = 0$.

$x = 0$. Consequently, one can pay attention to $\partial p / \partial x$ within $[0, 0.5]$, which shows both monotonic and non-monotonic nature depending on the parameters. The non-monotonic nature of $\partial p / \partial x$ indicates the development of an adverse pressure gradient that causes eddy structure formation due to the flow separation. The adverse pressure gradient is developed mainly due to the exchange of kinetic energy between AC and IF due to significant IF viscosity variation caused after fluid injection. This adverse pressure gradient leads to the creation of secondary eddy within the lifted portion of the SCL. We have discussed earlier that these eddies are helpful for better blending of injected fluid-containing drugs within IF. The pressure gradient becomes maximum at the line of injection. The next possible location having a low magnitude of the pressure gradient is the SM interface. Therefore, the SD interface experiences the lowest gradient of pressure.

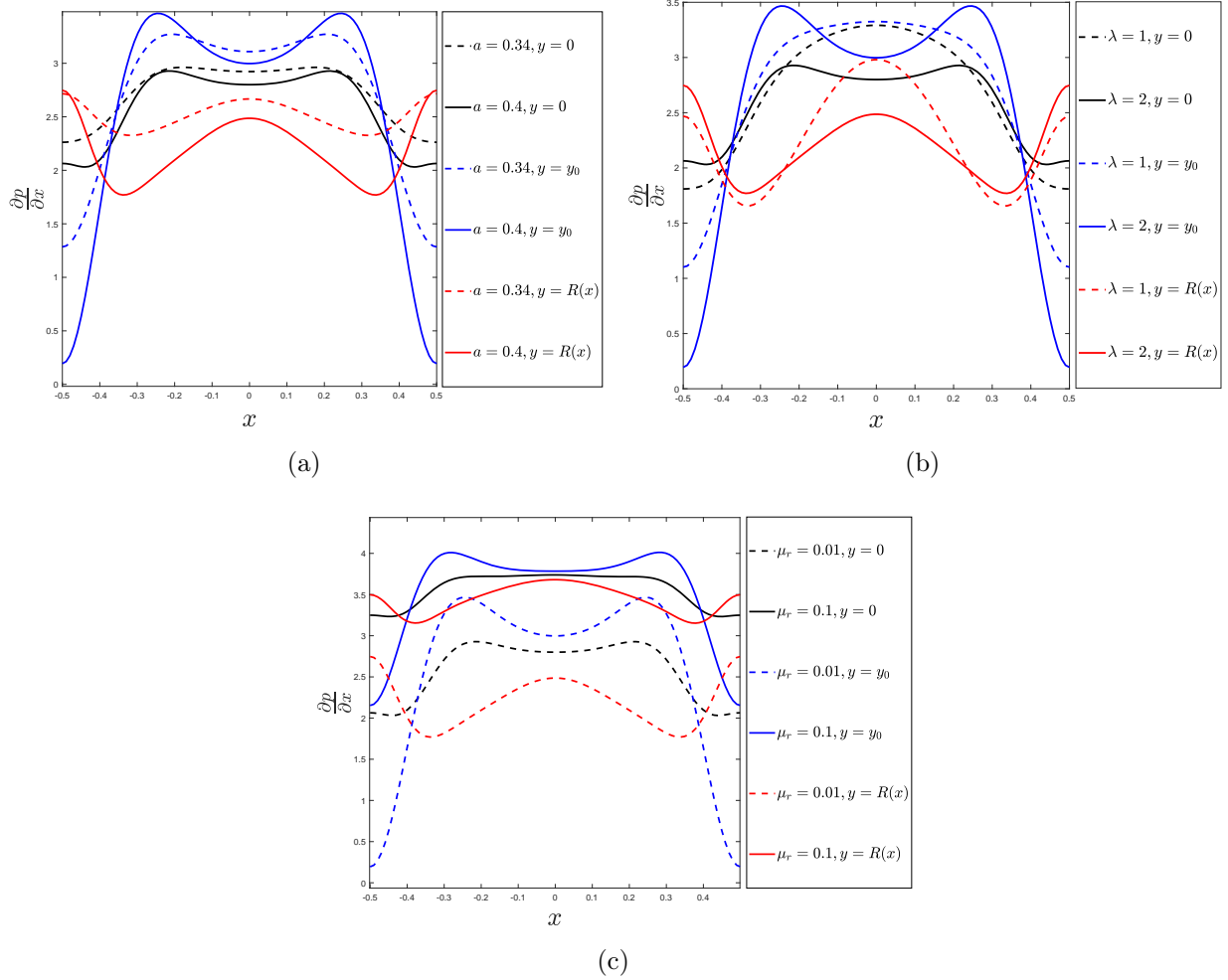


Figure 8: The pressure gradient variation with x , ($x \in [-0.5, 0.5]$) corresponding to (a) $a = 0.34, 0.4$ (b) $\lambda = 1, 2$ (c) $\mu_r = 0.01, 0.1$ at three locations $y = 0$ (SM interface), $y = y_0$ (line of injection), and $y = R(x)$ (SD interface).

On the other hand, the calculated shear stress as given by

$$\tau_{xy} = \frac{\partial u}{\partial y} + \delta^2 \frac{\partial v}{\partial x}, \quad (54)$$

behaves non-monotonic for $x \in [-0.5, 0.5]$ at the three distinct positions $y = y_0$ (line of injection), $y = 0$ (SM interface) and $y = R(x)$ (SD interface) (see Figs 9(a)-9(c)). Similar to the pressure gradient, as shown in the Figs 9(a)-9(c) the shear stress is also symmetric about $x = 0$ within $[-0.5, 0.5]$. The non-monotonic behavior of shear stress tends to display large fluctuation for $x \in [-0.5, 0.5]$ at $y = y_0$. But, such a high fluctuation never occurs for the other two positions of y . However, the SM interface experiences larger average shear

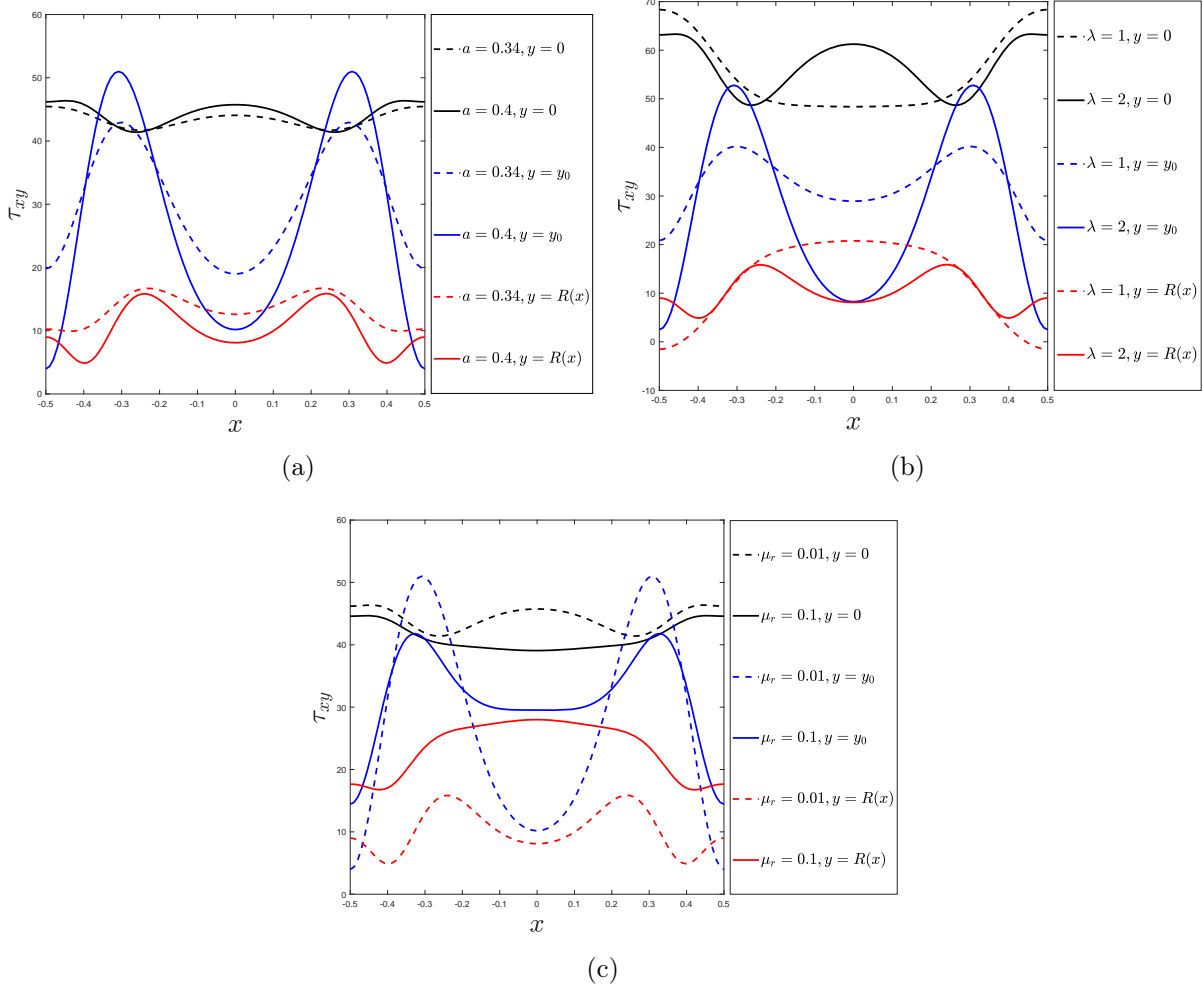


Figure 9: Shear stress profiles for (a) $a = 0.34, 0.4$ (b) $\lambda = 1, 2$ (c) $\mu_r = 0.01, 0.1$ at three locations $y = 0$ (SM interface), $y = y_0$ (line of injection), and $y = R(x)$ (SD interface).

stress than both the line of injection and SD interface. In addition, between SD and SM interfaces, the shear stress behaves exactly opposite each other. The behavioral difference of the shear stress fields between the SD interface and the line of injection allows the generation of secondary eddy from the primary one. On the other hand, the high shear stress close to the SM interface does not allow eddy formation. Hence, the formation of secondary eddy takes place near the SD interface only. Eventually, it can be said that the larger pressure gradient at $y = y_0$ and larger average shear stress at $y = 0$ help the injected fluid to move away from the line of injection and consequently lateral spreading of injected fluid at the SM interface due to the consideration of slip property.

The fluctuation in the non-monotonic profile of both the pressure gradient and shear stress profile corresponding to $y = y_0$ becomes pronounced with an increase in the depth of SCL

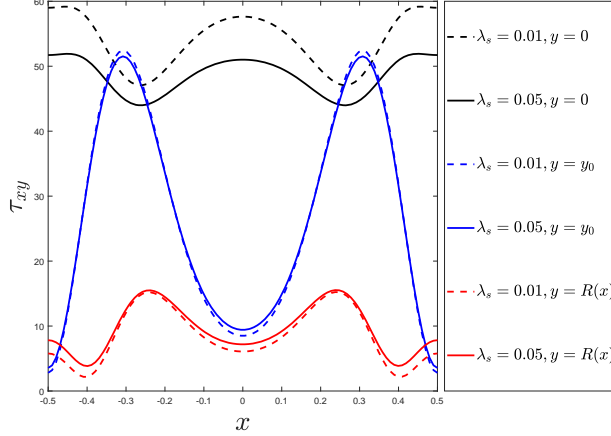


Figure 10: Shear stress variation with $x \in [-0.5, 0.5]$ for $\lambda_s = 0.01, 0.05$ and at three different locations (i) SM interface ($y = 0$) (ii) line of injection ($y = y_0$) (iii) SD interface ($y = R(x)$).

pinched up. But at the other two positions, such high fluctuation cannot be seen. Moreover, it is noticed that pressure gradient and shear stress reduce with the increase in the depth of SCL pinched up during injection. However, it is rather difficult to predict anything from Figs. 8(a) and 9(a) about the variations of a on both the pressure gradient and shear stress at $y = 0$ and $y = y_0$. On the other hand, the impact of a on both the pressure gradient and shear stress can be easily understood at $y = R(x)$ (SD interface). Therefore at this moment, we may focus on the SD interface only. Now, suppose we associate the experience of the intensity of pain with the variation of pressure gradient and shear stress. In that case, we find that a patient may realize less pain from the SD interface for a higher depth of skin pinching during the injection.

The tissue anisotropy destroys the monotonic nature of the profiles of both the shear stress and pressure gradient as depicted through the Figs. 8(b) and 9(b). In other words, higher λ (more precisely for all possible $\lambda > 1$) imparts fluctuation in the pressure gradient and shear stress profiles. In particular for $\lambda = 2$, the profiles of $\partial p/\partial x$ at $y = y_0$ and $y = R(x)$ behave exactly opposite to each other. This opposite behavior of $\partial p/\partial x$ is responsible for creation of secondary eddy from the primary one. In addition, we notice that at $y = 0$ and $y = y_0$, $\partial p/\partial x$ maintains monotonic nature for $\lambda = 1$ (isotropic). This monotonic nature changes to non-monotonic with increased λ beyond 1 (adverse pressure gradient is developed). At the three positions, average magnitude of $\partial p/\partial x$ reduces with increase in anisotropy. Hence, one would expect less pain generation from those sites due to increased anisotropy. On the other hand, the development of larger shear stress at the SM interface with increased λ may consequence a patient to realize more pain generated from the SM interface though $\partial p/\partial x$ reduces with increase in λ . Also at $y = y_0$, an increase in the shear stress is noted with the increased anisotropy. But at the SD interface, the average shear stress reduces with increase in λ beyond 1. Like $\partial p/\partial x$, the shear stress changes its nature from monotonic to non-monotonic with increased tissue anisotropy. From the overall discussions, it is seen that

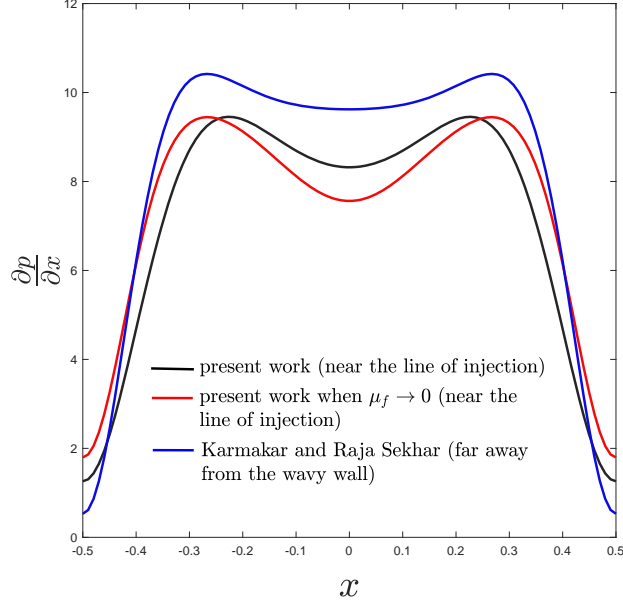


Figure 11: Comparison of pressure gradients obtained (i) from the present study (black line) near the line $y = y_0$ (line of injection), (ii) in the limiting case $\mu_f \rightarrow 0$ (red line) close to the line of injection (see Eq.(61)) and (iii) from the study of Karmakar and Raja Sekhar [45] which discusses the hydrodynamics of fluid flow through a wavy anisotropic porous channel (blue line).

both $\partial p/\partial x$ and shear stress reduces with increase in λ beyond the isotropic limit. Hence, a patient may experience less pain in the form of superficial pain from the SD interface when the SCL possesses significant larger anisotropy.

Both the pressure gradient and shear stress significantly vary with the viscosity of injected drug. Figs. 8(c) and 9(c) illustrate pressure gradient and shear stress for $\mu_r = 0.01$ and $\mu_r = 0.1$ corresponding to three locations $y = 0$, $y = y_0$ and $y = R(x)$ while other parameters are $a = 0.4$, $\lambda = 2$, $\lambda_s = 0.05$ and $y_0 = 0.45$. We observe the rise of $\partial p/\partial x$ with the increasing magnitude of μ_r in the above three locations of y . Since $\lambda = 2$ (consideration anisotropic permeability of SCL), a non-monotonic nature of both $\partial p/\partial x$ and shear stress is observed. This behavior becomes more aggressive with decreasing μ_r . Therefore, upon injecting a low viscous fluid (much lower as compared to the AC), we can achieve such high non-monotonic behavior in $\partial p/\partial x$. Moreover, corresponding to $\mu_r = 0.01$, once again the opposite behavior of $\partial p/\partial x$ is noticed between the positions $y = y_0$ and $y = R(x)$. This will guarantee the formation of secondary eddy from the primary one.

Further, we focus on the shear stress distribution for $\mu_r = 0.01, 0.1$ at the three locations $y = 0$, $y = y_0$ and $y = R(x)$ when the other parameters are fixed as above. As analogous to the impact of pressure gradient, low μ_r shows sensitivity towards the shear stress field. The response of the shear stress field is not much significant near the SM interface (i.e, near

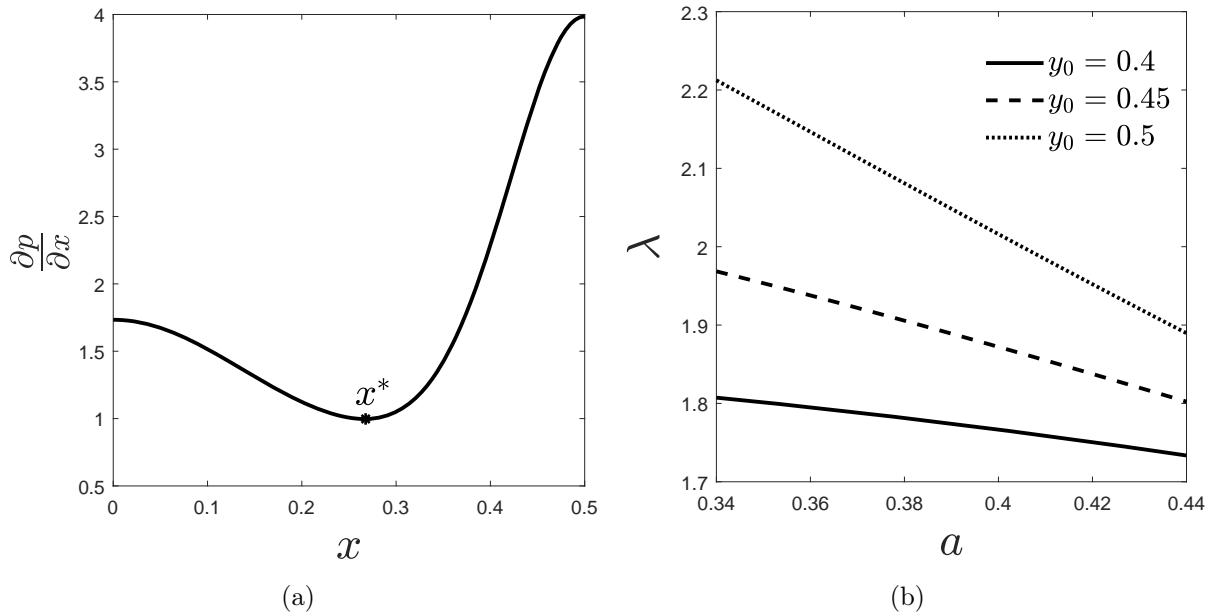


Figure 12: (a) Pressure gradient variation with respect to $x \in [0, 0.5]$; x^* is the optimum value point, (b) Anisotropic ratio (λ) versus a for $y_0 = 0.4, 0.45, 0.5$.

$y = 0$). However, near the line of injection (i.e, $y = y_0$) the increased non-monotonicity in the shear stress profile is noted due to reduced μ_r . It is expected that this sensitivity (increase in non-monotonicity) becomes even higher in case of further lower μ_r . On the other hand, an increased magnitude of $\partial p/\partial x$ and shear stress can be noted at the SD interface with increase in μ_r from 0.01 to 0.1. This incident predicts the enhancement of superficial pain when a high viscous fluid is injected within SCL. Injection of low viscous fluid leads to both primary and secondary eddies as a consequence of the rapid change in the shear stress field between $y = 0$ and $y = y_0$ and between $y = y_0$ and $y = R(x)$ respectively. Consequently, from the observations of pressure gradient and shear stress field we may conclude that besides the higher tissue anisotropy ($\lambda \geq 1.75$), a larger difference in viscosity between the injected fluid and AC (i.e., $\mu_r < 0.05$) causes adequate circulation of the injected fluid within the interstitial space of SCL.

4.4 Effect of slip coefficient λ_s on shear stress

Since the slip coefficient λ_s is proportional to \sqrt{Da} , it characterizes the material property of the SM interface while responding to the generated shear stress during the fluid injection process. The effect of λ_s on shear stress is distributed perpendicular to the other portions of SCL as well. With ageing SCL becomes thin and develops rigidity (Da may assume smaller value). As a result, SM interface also attains higher rigidity. This suggests λ_s to assume smaller value as compared to lesser rigid SM interface. On the other hand, a low/middle aged or healthy person develops relatively low shear stress at the SM interface. Consequently, λ_s

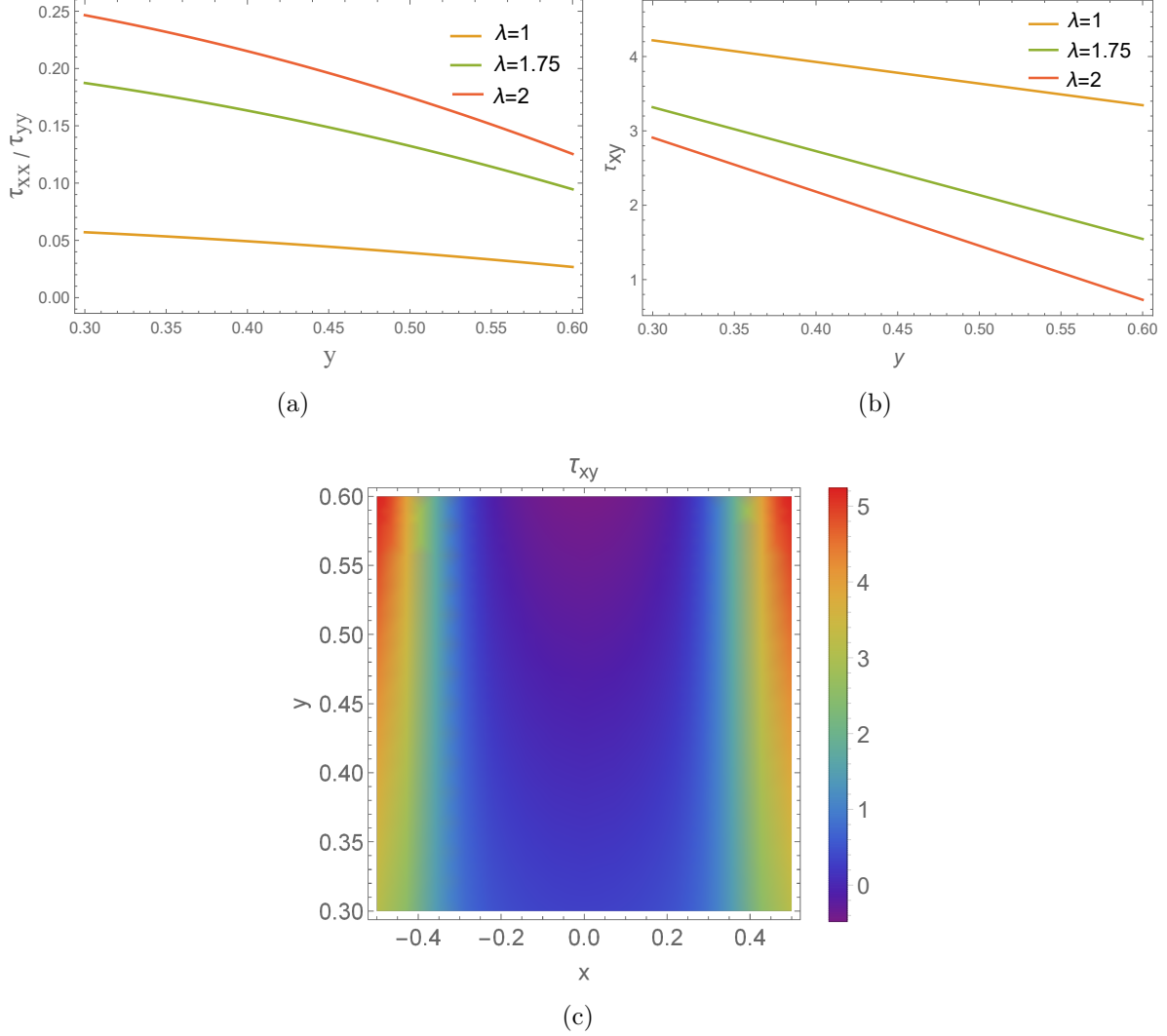


Figure 13: (a) Normal stress components τ_{xx} & τ_{yy} , (b) shear stress τ_{xy} for $\lambda = 1, 1.75, 2$ and (c) shear stress field within the domain $\{(x, y) : -0.5 \leq x \leq 0.5, 0.3 \leq y \leq 0.6\}$ corresponding to $\lambda = 2$.

assumes its larger magnitude as compared to the case of a thin or aged person. Based on the choice of Da in this present study, we need $\lambda_s > 0$ and can be chosen $\lambda_s = 0.01, 0.05$. Fig. (10) elucidates that the SM interface is more sensitive to the shear stress developed as compared to the other portion of SCL. As λ_s controls the shear stress at the SM interface, high shear stress is noted at the SM interface at a low magnitude of λ_s (e.g., $\lambda_s = 0.01$). The developed shear stress gets dissipated along the interface when λ_s is high (e.g., $\lambda_s = 0.05$). In the other words, the SCL acts as a shear stress absorber when λ_s is large and saves the underlying ML from possible damage due to the stress. Hence, at higher λ_s , a patient may realize less pain as a result of shear stress dissipation. Consequently, high λ_s induces a favorable situation by reducing the shear stress during fluid injection. With the ageing, the

subcutaneous injection losses some of its benefits and develop chance of lasting pain to the patient. However, to a healthy or a young aged people, the developed pain may be lasted for less time.

4.5 Hydrodynamic behaviour near the line of injection

We anticipate that the viscous force becomes negligible near the line of injection within the SC layer due to the weakening impact of the hydrodynamic boundary layer. One can compare this situation with the significant domination of viscous forces close to the wall for a Poiseuille type flow within a channel or tube. Moreover, such domination is found to be relevant in the case of Poiseuille type flow in fluid overlying a porous medium [62] and 2D flow through a wavy anisotropic porous channel [45] where flows near the boundary obeys the Brinkman equation but are far from the boundary viscous forces become less effective and hence the flow satisfies Darcy equation. Consequently in this study, the second-order derivative terms in the momentum equation for the IF motion and the terms containing μ_f/μ_c can be dropped. Subsequently, we obtain the following equations for the leading order:

$$(u_{f_0} - u_{c_0}) \sim -\frac{\partial p_0}{\partial x}, \quad (55)$$

and

$$(v_{f_0} - v_{c_0}) \sim \frac{\partial^2 p_0}{\partial x^2} y. \quad (56)$$

From the volumetric flow rate balance, one can obtain the pressure gradient for leading order as

$$p_{0x} \sim \left(\frac{R(x)}{2} - \frac{1}{R(x)} \right). \quad (57)$$

Similarly, we can obtain the $O(\delta^2)$ equations as

$$(u_{f_1} - u_{c_1}) \sim \lambda^2 \frac{p_{0xxx}}{2} y^2 + d_1(x), \quad (58)$$

and consequently, using the volumetric flow rate across the cross section, $d_1(x)$ is determined as

$$d_1(x) \sim -\lambda^2 \frac{p_{0xxx}}{6} R^2(x) - \frac{R(x)}{2}. \quad (59)$$

Finally, we have the pressure gradient for $O(\delta^2)$ as

$$p_{1_x} \sim -\lambda^2 \frac{p_{0xxx}}{2} \left(y^2 - \frac{R(x)^2}{3} \right) + \frac{R(x)}{2}. \quad (60)$$

Thus, the pressure gradient up to $O(\delta^2)$ is

$$\frac{\partial p}{\partial x} \sim \frac{\partial p_0}{\partial x} - \delta^2 \lambda^2 \frac{p_{0xxx}}{2} \left(y^2 - \frac{R(x)^2}{3} \right) + \frac{\delta^2}{2} R(x). \quad (61)$$

The utility of the above analysis aims to deduce the normal and tangential stresses in a convenient way (without involving tedious calculations). Hence to check the validity, we can compare the pressure gradient as in Eq. (61) with that of obtained from the main calculations near the line of injection (or far away from the interfaces). Therefore through Fig. 11, we observe that both the pressure gradients show similar behavior both qualitative and quantitative points of view (black and red lines). We can also establish the validity of the present model by plotting the pressure gradient obtained from the study of Karmakar and Raja Sekhar [45] corresponding to the fixed anisotropy ratio $\lambda = 2$. The blue line represents the pressure gradient variation versus x showing a nice qualitative agreement with the present study. Note that the anisotropic geometry is the key feature of both the studies.

From the Eq. (61), we have the pressure gradient near the line injection. In particular, at the line of injection

$$\frac{\partial p}{\partial x} = p_{0x} - \delta^2 \lambda^2 \frac{p_{0xxx}}{2} \left(y_0^2 - \frac{R(x)^2}{3} \right) + \frac{\delta^2}{2} R(x). \quad (62)$$

Pressure gradient from Eq. (62) may attain its optimum value at some points which can be calculated. If x^* denote such an optimum point (see Fig. (12(a))), then we have

$$\lambda^2 \delta^2 \left(\frac{p_{0xxxx}(x^*)}{2} \left(y_0^2 - \frac{R(x^*)^2}{3} \right) - \frac{p_{0xxx}(x^*)}{3} R(x^*) R'(x^*) \right) = p_{0xx}(x^*) + \frac{\delta^2}{2} R'(x^*) \quad (63)$$

Eq. (63) gives an explicit relation between the anisotropic ratio λ , amplitude a and penetration depth y_0 (height of the line of injection from SM interface). As tissue anisotropy is a material property, it can not be controlled from outside by an administrator during injection, though the pinching depth a and penetration depth $(1 - y_0)$ can be regulated during the injection time. So it would be very effective if we find a relation between λ , a and y_0 . In this context, Eq. (63) gives an idea about λ in terms of a and y_0 . Consequently, Fig. 12(b) shows variation of anisotropic ratio λ with respect to amplitude a corresponding to the different penetration depth $y_0 = 0.4, 0.45$ and 0.5 . It is evident that with the increase of a , λ decreases along the injection line y_0 . Even when skin pinching is high, and tissue anisotropy is relatively low, eddies can still form and assist in adequately mixing the injected fluid with IF. Moreover, tissue anisotropy increases as the injection line moves deeper into the tissue. This implies that higher injection depths may necessitate higher levels of tissue anisotropy compared to other cases.

Fig. 13(a) represents normal stresses τ_{xx} and τ_{yy} for various λ within the range $0.3 \leq y \leq 0.6$ enclosing the line of injection. We observe that the normal stresses increase with λ . Therefore both along the x and y directions, the intensity of the pain at the injection site increases with tissue anisotropy. On the other hand, Fig. 13(b) shows opposite behaviour corresponding to that of shear stress variation concerning λ within the above range of y . The pain generated due to the shear stress decreases with increasing tissue anisotropy. The inverse behavior of normal and shear stress fields maintains the mechanical equilibrium within the SC layer which

becomes imbalanced due to the tissue anisotropy variation. The behavior of the shear stress field can be justified from the longitudinal pressure gradient ($\partial p/\partial x$) variations concerning y for various λ near the line of injection. The rate of shear stress variation along the direction normal to the line of injection is proportional to $\partial p/\partial x$. Moreover from Fig. 13(c), one can notice the behaviour of shear stress in the domain $\{(x, y) : -0.5 \leq x \leq 0.5, 0.3 \leq y \leq 0.6\}$ containing the line of injection. It shows that the magnitude of shear stress is symmetric with respect to x -axis. The minimum value of shear stress attained at $x = 0$. In other words, shear stress attains its minimum value at the position where the skin is being lifted up. The injected drug spreads from the injection point to the extracellular region. Consequently, shear stress is developed away from the line $x = 0$.

5 Concluding Remarks

A two-dimensional fluid injection model within the subcutaneous layer (SCL) has been investigated using biphasic mixture theory. We study the flow pattern of the injected fluid (containing drug), pressure gradient, and shear stress in terms of parameters a (skin pinching height), λ (anisotropy ratio), μ_r (viscosity ratio), and λ_S (slip coefficient). The overall hydrodynamic analysis reveals the creation of the primary eddy structure at the line of injection due to the development of a high-pressure gradient. In addition, it is seen that the lifted portion of the SCL may witness secondary eddies depending on the viscosity of the injected fluid and the height of the skin pinching. Depending on the anisotropy ratio, one may see this secondary eddy if the SD interface is not regular. Both the primary and secondary eddies play a significant role to homogenize the injected fluid with the IF when (i) the anisotropy ratio of SCL is greater than 1.5 (ii) low viscosity ratio ($\mu_r < 0.05$) and (iii) high skin pinching height ($a > 0.3$).

Since pressure gradient and shear stress act as possible indicators of pain generation inside SCL [68, 69], the high viscous injected fluid may induce pain to a patient receiving SCI. On the other hand, our analysis reveals that low skin pinching height and small anisotropy ratio of SCL can be held responsible for realizing of more pain. Moreover, the shear stress at the SM interface is high corresponding to a small slip coefficient ($\lambda_s = 0.001$). Thus, the SCL can affect the underlying ML by imparting high shear stress generated from the fluid injection. With the ageing issue, enhanced shear stress is developed at the SM interface which is manifested by a smaller slip coefficient ($\lambda_s \leq 0.001$).

Acknowledgements

First author A. S. Pramanik acknowledges University Grants Commission (UGC), Govt. of India for providing junior research fellowship (NET-JRF, Award Letter Number: 1149/(CSIR-UGC NET DEC-2018)). Second author B. Dey acknowledges University research assistance (Ref. 1516/R-2020 dated 01.06.2020) of University of North Bengal for supporting this work.

Authors are very much thankful to Prof. G. P. Raja Sekhar, Professor of Mathematics at Indian Institute of Technology Kharagpur, West Bengal, India, for his inspiration and necessary comments to improve this manuscript.

Appendix A. Solution to the leading-order problem

With the boundary conditions, the solution of the equations (27)-(31) are

$$u_{f_0}(x, y) = \frac{X_0(x, y) + Y_0(x, y)}{1 + \mu_r}, \quad u_{c_0}(x, y) = \frac{X_0(x, y) - \mu_r Y_0(x, y)}{1 + \mu_r},$$

where $X_0(x, y)$ and $Y_0(x, y)$ are given by

$$X_0(x, y) = \begin{cases} L_1 p_{0x} y^2 + A_1^{(0)}(x) y + A_2^{(0)}(x), & \text{if } 0 < y < y_0 \\ L_1 p_{0x} (R(x) - y)^2 + A_3^{(0)}(x) (R(x) - y) + A_4^{(0)}(x), & \text{if } y_0 < y < R(x) \end{cases}$$

$$Y_0(x, y) = \begin{cases} B_1^{(0)}(x) \cosh(\beta y) + B_2^{(0)}(x) \sinh(\beta y) + L_2 p_{0x}, & \text{if } 0 < y < y_0 \\ B_3^{(0)}(x) \cosh(\beta(R(x) - y)) + B_4^{(0)}(x) \sinh(\beta(R(x) - y)) + L_2 p_{0x}, & \text{if } y_0 < y < R(x) \end{cases}$$

in which $A_i^{(0)}(x)$, $B_i^{(0)}(x)$ ($i = 1, 2, 3, 4$) are constants of integration which can be calculated using the boundary conditions with the condition of continuity at $y = y_0$. L_1 , L_2 and β are given by the followings

$$L_1 = \frac{\mu_r \alpha^2}{2}, \quad L_2 = -\frac{(\phi_f - \phi_c \mu_r)}{1 + \mu_r} \quad \text{and} \quad \beta^2 = (1 + \mu_r) \alpha^2.$$

Also using the equation of continuity, we have

$$v_{f_0}(x, y) = \frac{V_0(x, y) + W_0(x, y)}{1 + \mu_r}, \quad v_{c_0}(x, y) = \frac{V_0(x, y) - \mu_r W_0(x, y)}{1 + \mu_r},$$

where $V_0(x, y)$ and $W_0(x, y)$ are given by

$$V_0(x, y) = \begin{cases} -\frac{1}{3} L_1 p_{0xx} y^3 - \frac{1}{2} \left(A_1^{(0)}(x) \right)_x y^2 - \left(A_2^{(0)}(x) \right)_x y + c_1^{(0)}(x), & \text{if } 0 < y < y_0 \\ -\frac{1}{3} L_1 p_{0xx} (R(x) - y)^3 - \frac{1}{2} \left(A_3^{(0)}(x) \right)_x (R(x) - y)^2 \\ - \left(A_4^{(0)}(x) \right)_x (R(x) - y) + c_2^{(0)}(x), & \text{if } y_0 < y < R(x) \end{cases}$$

$$W_0(x, y) = \begin{cases} -\frac{1}{\beta} \left(B_1^{(0)}(x) \right)_x \sinh(\beta y) - \frac{1}{\beta} \left(B_2^{(0)}(x) \right)_x \cosh(\beta y) - L_2 p_{0xx} y + d_1^{(0)}(x), & \text{if } 0 < y < y_0 \\ -\frac{1}{\beta} \left(B_3^{(0)}(x) \right)_x \sinh(\beta(R(x) - y)) - \frac{1}{\beta} \left(B_4^{(0)}(x) \right)_x \cosh(\beta(R(x) - y)) \\ -L_2 p_{0xx}(R(x) - y) + d_2^{(0)}(x), & \text{if } y_0 < y < R(x) \end{cases}$$

in which $c_i^{(0)}(x)$, $d_i^{(0)}(x)$ ($i = 1, 2$) are constants of integration which can be calculated using the boundary conditions.

Appendix B. Solution to the $O(\delta^2)$ problem

The general solution of the $O(\delta^2)$ problem is

$$u_{f_1}(x, y) = \frac{X_1(x, y) + Y_1(x, y)}{1 + \mu_r}, \quad u_{c_1}(x, y) = \frac{X_1(x, y) - \mu_r Y_1(x, y)}{1 + \mu_r},$$

where $X_1(x, y)$ and $Y_1(x, y)$ are given by

$$X_1(x, y) = \begin{cases} E_1(x)y^4 + E_2(x)y^3 + E_3(x)y^2 + A_1^{(1)}(x)y^2 + A_2^{(1)}(x)y + A_3^{(1)}(x), & \text{if } 0 < y < y_0 \\ E_1(x)(R(x) - y)^4 + E_4(x)(R(x) - y)^3 + E_5(x)(R(x) - y)^2 \\ + A_1^{(1)}(x)(R(x) - y)^2 + A_4^{(1)}(x)(R(x) - y) + A_5^{(1)}(x), & \text{if } y_0 < y < R(x) \end{cases}$$

$$Y_1(x, y) = \begin{cases} B_1^{(1)}(x) + B_2^{(1)}(x)\cosh(\beta y) + B_3^{(1)}(x)\sinh(\beta y) + F_1(x)y\sinh(\beta y) \\ + F_2(x)y\cosh(\beta y) + F_3(x)(\beta^2 y^2 + 2) + F_4(x)y + F_5(x), & \text{if } 0 < y < y_0 \\ B_1^{(1)}(x) + B_4^{(1)}(x)\cosh(\beta(R(x) - y)) + B_5^{(1)}(x)\sinh(\beta(R(x) - y)) \\ + F_6(x)(R(x) - y)\sinh(\beta(R(x) - y)) + F_7(x)(R(x) - y)\cosh(\beta(R(x) - y)) \\ + F_3(x)(\beta^2(R(x) - y)^2 + 2) + F_8(x)(R(x) - y) + F_5(x), & \text{if } y_0 < y < R(x) \end{cases}$$

in which $A_i^{(1)}(x)$, $B_i^{(1)}(x)$ ($i = 1, 2, 3, 4, 5$) are constants of integration which can be calculated using the boundary conditions and condition of continuity at $y = y_0$. $E_i(x)$ ($i = 1, 2, 3, 4, 5$) and $F_i(x)$ ($i = 1, 2, 3, 4, 5, 6, 7, 8$) are explicitly given in the Appendix C.

Hence, the general solution of the considered problem is determined upto $O(\delta^2)$ as

$$u_f(x, y) = u_{f_0}(x, y) + \delta^2 u_{f_1}(x, y) + O(\delta^4),$$

$$u_c(x, y) = u_{c_0}(x, y) + \delta^2 u_{c_1}(x, y) + O(\delta^4).$$

Appendix C.

$$\begin{aligned} E_1(x) &= -\frac{1}{6}L_1p_{0xxx}, & E_2(x) &= -\frac{1}{3}(A_1^{(0)}(x))_{xx}, & E_3(x) &= -(A_2^{(0)}(x))_{xx}, \\ E_4(x) &= -\frac{1}{3}(A_3^{(0)}(x))_{xx}, & E_5(x) &= -(A_4^{(0)}(x))_{xx}, & F_1(x) &= \frac{(\lambda^2-2)}{2\beta}(B_1^{(0)}(x))_{xx}, \\ F_2(x) &= \frac{(\lambda^2-2)}{2\beta}(B_2^{(0)}(x))_{xx}, & F_3(x) &= \frac{\lambda^2}{2\beta^2}L_2p_{0xxx}, & F_4(x) &= \lambda^2(d_1^{(0)}(x))_x, \\ F_5(x) &= -\frac{2}{\beta^2}L_2p_{0xxx}, & F_6(x) &= \frac{(\lambda^2-2)}{2\beta}(B_3^{(0)}(x))_{xx}, & F_7(x) &= \frac{(\lambda^2-2)}{2\beta}(B_4^{(0)}(x))_{xx}, \\ F_8(x) &= \lambda^2 \left(d_2^{(0)}(x) \right)_x. \end{aligned}$$

References

- [1] Hyejeong Kim, Hanwook Park, and Sang Joon Lee. Effective method for drug injection into subcutaneous tissue. *Scientific Reports*, 7(1):1–11, 2017.
- [2] Sherri Ogston-Tuck. Subcutaneous injection technique: an evidence-based approach. *Nursing Standard*, 29(3):53–58, 2014.
- [3] Samuel S Dychter, David A Gold, and Michael F Haller. Subcutaneous drug delivery: a route to increased safety, patient satisfaction, and reduced costs. *Journal of Infusion Nursing*, 35(3):154–160, 2012.
- [4] Ralph S Shapiro. Why i use subcutaneous immunoglobulin (scig). *Journal of Clinical Immunology*, 33(2):95–98, 2013.
- [5] Loyd Allen and Howard C Ansel. Ansel’s pharmaceutical dosage forms and drug delivery systems. *American Journal of Pharmaceutical Education*, 70(3):X1, 2013.
- [6] Julie Prettyman. Subcutaneous or intramuscular? confronting a parenteral administration dilemma. *Medsurg Nursing*, 14(2):93–99, 2005.
- [7] Kelly L Stoner, Helena Harder, Lesley J Fallowfield, and Valerie A Jenkins. Intravenous versus subcutaneous drug administration. which do patients prefer? a systematic review. *The Patient-Patient-Centered Outcomes Research*, 8(2):145–153, 2015.
- [8] Michael F Haller. Converting intravenous dosing to subcutaneous dosing with recombinant human hyaluronidase. *Pharmaceutical Technology*, 31(10), 2007.
- [9] Marion Geerligs, Gerrit W M Peters, Paul A J Ackermans, Cees W J Oomens, and Frank Baaijens. Linear viscoelastic behavior of subcutaneous adipose tissue. *Biorheology*, 45(6):677–688, 2008.
- [10] Kerstyn Comley and Norman Fleck. Deep penetration and liquid injection into adipose tissue. *Journal of Mechanics of Materials and Structures*, 6(1):127–140, 2011.

- [11] S Derler and L-C Gerhardt. Tribology of skin: review and analysis of experimental results for the friction coefficient of human skin. *Tribology Letters*, 45(1):1–27, 2012.
- [12] Pranav Shrestha and Boris Stoeber. Fluid absorption by skin tissue during intradermal injections through hollow microneedles. *Scientific Reports*, 8(1):1–13, 2018.
- [13] Pranav Shrestha and Boris Stoeber. Imaging fluid injections into soft biological tissue to extract permeability model parameters. *Physics of Fluids*, 32(1):011905, 2020.
- [14] S I Barry and G K Aldis. Flow-induced deformation from pressurized cavities in absorbing porous tissues. *Bulletin of Mathematical Biology*, 54(6):977–997, 1992.
- [15] C W J Oomens, D H Van Campen, and H J Grootenboer. A mixture approach to the mechanics of skin. *Journal of Biomechanics*, 20(9):877–885, 1987.
- [16] Clifford Truesdell and Richard Toupin. *The Classical Field Theories*. Springer, 1960.
- [17] Kumbakonam R Rajagopal and Luoyi Tao. *Mechanics of Mixtures*, volume 35. World Scientific, 1995.
- [18] Clifford Truesdell, Walter Noll, C Truesdell, and W Noll. *The Non-linear Field Theories of Mechanics*. Springer, 2004.
- [19] KR Rajagopal, AS Wineman, and M Gandhi. On boundary conditions for a certain class of problems in mixture theory. *International Journal of Engineering Science*, 24(8):1453–1463, 1986.
- [20] MV Gandhi, KR Rajagopal, and AS Wineman. Some nonlinear diffusion problems within the context of the theory of interacting continua. *International Journal of Engineering Science*, 25(11-12):1441–1457, 1987.
- [21] A Wineman and Kumbakonam R Rajagopal. Shear induced redistribution of fluid within a uniformly swollen nonlinear elastic cylinder. *International Journal of Engineering Science*, 30(11):1583–1595, 1992.
- [22] Helen Byrne and Luigi Preziosi. Modelling solid tumour growth using the theory of mixtures. *Mathematical Medicine and Biology: A Journal of the IMA*, 20(4):341–366, 2003.
- [23] Kumbakonam R Rajagopal. On a hierarchy of approximate models for flows of incompressible fluids through porous solids. *Mathematical Models and Methods in Applied Sciences*, 17(02):215–252, 2007.
- [24] Prakash Kumar, Bibaswan Dey, and G P Raja Sekhar. Nutrient transport through deformable cylindrical scaffold inside a bioreactor: an application to tissue engineering. *International Journal of Engineering Science*, 127:201–216, 2018.

- [25] Bibaswan Dey and G P Raja Sekhar. Mathematical modeling of electrokinetic transport through endothelial-cell glycocalyx. *Physics of Fluids*, 33(8):081902, 2021.
- [26] Marcelino Anguiano, Arif Masud, and Kumbakonam R Rajagopal. Mixture model for thermo-chemo-mechanical processes in fluid-infused solids. *International Journal of Engineering Science*, 174:103576, 2022.
- [27] Helen M Byrne, John R King, D L Sean McElwain, and Luigi Preziosi. A two-phase model of solid tumour growth. *Applied Mathematics Letters*, 16(4):567–573, 2003.
- [28] Christopher J W Breward, Helen M Byrne, and Claire E Lewis. A multiphase model describing vascular tumour growth. *Bulletin of Mathematical Biology*, 65(4):609–640, 2003.
- [29] Kumbakonam Ramamani Rajagopal. Mechanics of liquid mixtures. In *Rheology of Complex Fluids*, pages 67–84. Springer, 2010.
- [30] C Y Chen, H M Byrne, and J R King. The influence of growth-induced stress from the surrounding medium on the development of multicell spheroids. *Journal of Mathematical Biology*, 43(3):191–220, 2001.
- [31] S I Barry and G K Aldis. Comparison of models for flow induced deformation of soft biological tissue. *Journal of Biomechanics*, 23(7):647–654, 1990.
- [32] S I Barry, K H Parkerf, and G K Aldis. Fluid flow over a thin deformable porous layer. *Zeitschrift für Angewandte Mathematik und Physik ZAMP*, 42(5):633–648, 1991.
- [33] Steven I Barry, Geoffrey K Aldis, and Geoffry N Mercer. Injection of fluid into a layer of deformable porous medium. *Applied Mechanics Reviews*, 40(10):722–726, 1995.
- [34] S I Barry, G N Mercer, and C Zoppou. Deformation and fluid flow due to a source in a poro-elastic layer. *Applied Mathematical Modelling*, 21(11):681–689, 1997.
- [35] Jiayu Li and James D Johnson. Mathematical models of subcutaneous injection of insulin analogues: a mini-review. *Discrete and Continuous Dynamical Systems. Series B*, 12(2):401, 2009.
- [36] Van C. Mow, Mark H Holmes, and W Michael Lai. Fluid transport and mechanical properties of articular cartilage: a review. *Journal of Biomechanics*, 17(5):377–394, 1984.
- [37] Mark H Holmes. A theoretical analysis for determining the nonlinear hydraulic permeability of a soft tissue from a permeation experiment. *Bulletin of Mathematical Biology*, 47(5):669–683, 1985.
- [38] H H Wei, S L Waters, Shu Qian Liu, and J B Grotberg. Flow in a wavy-walled channel lined with a poroelastic layer. *Journal of Fluid Mechanics*, 492:23–45, 2003.

- [39] Bibaswan Dey and G P Raja Sekhar. Hydrodynamics and convection enhanced macromolecular fluid transport in soft biological tissues: Application to solid tumor. *Journal of Theoretical Biology*, 395:62–86, 2016.
- [40] D Andrew S Rees and L Storesletten. The effect of anisotropic permeability on free convective boundary layer flow in porous media. *Transport in Porous Media*, 19(1):79–92, 1995.
- [41] L E Payne, J F Rodrigues, and B Straughan. Effect of anisotropic permeability on darcy’s law. *Mathematical Methods in the Applied Sciences*, 24(6):427–438, 2001.
- [42] Timir Karmakar and G P Raja Sekhar. Effect of anisotropic permeability on convective flow through a porous tube with viscous dissipation effect. *Journal of Engineering Mathematics*, 110(1):15–37, 2018.
- [43] D Rajani, V K Narla, and K Hemalatha. Anisotropic permeability impact on nanofluid channel flow (ch3oh-fe3o4) with convection. *Materials Today: Proceedings*, 28:2251–2257, 2020.
- [44] Mirela Kohr, G P Raja Sekhar, and John R Blake. Green’s function of the brinkman equation in a 2d anisotropic case. *IMA Journal of Applied Mathematics*, 73(2):374–392, 2008.
- [45] Timir Karmakar and G P Raja Sekhar. A note on flow reversal in a wavy channel filled with anisotropic porous material. *Proceedings of the Royal Society A: Mathematical, Physical and Engineering Sciences*, 473(2203):20170193, 2017.
- [46] Boris Reynaud and Thomas M Quinn. Anisotropic hydraulic permeability in compressed articular cartilage. *Journal of Biomechanics*, 39(1):131–137, 2006.
- [47] Salvatore Federico and Walter Herzog. On the anisotropy and inhomogeneity of permeability in articular cartilage. *Biomechanics and Modeling in Mechanobiology*, 7(5):367–378, 2008.
- [48] James C Iatridis, Lori A Setton, Robert J Foster, Bernard A Rawlins, Mark Weidenbaum, and Van C Mow. Degeneration affects the anisotropic and nonlinear behaviors of human annulus fibrosus in compression. *Journal of Biomechanics*, 31(6):535–544, 1998.
- [49] Salvatore Federico and Walter Herzog. On the permeability of fibre-reinforced porous materials. *International Journal of Solids and Structures*, 45(7-8):2160–2172, 2008.
- [50] Gerhard A Holzapfel et al. Biomechanics of soft tissue. *The Handbook of Materials Behavior Models*, 3(1):1049–1063, 2001.
- [51] E Shepherd. Injection technique 2: administering drugs via the subcutaneous route. *Nursing Times*, 114:55–57, 2018.

- [52] Bibaswan Dey and G P Raja Sekhar. A theoretical study on the elastic deformation of cellular phase and creation of necrosis due to the convection reaction process inside a spherical tumor. *International Journal of Biomathematics*, 9(06):1650095, 2016.
- [53] J S Barbieri, K Wanat, and J Seykora. Skin: basic structure and function. In *Pathobiology of Human Disease: A Dynamic Encyclopedia of Disease Mechanisms*, pages 1134–1144. Elsevier, 2014.
- [54] VL Savatorova and KR Rajagopal. Homogenization of a generalization of brinkman’s equation for the flow of a fluid with pressure dependent viscosity through a rigid porous solid. *ZAMM-Journal of Applied Mathematics and Mechanics/Zeitschrift für Angewandte Mathematik und Mechanik*, 91(8):630–648, 2011.
- [55] Bibaswan Dey and G P Raja Sekhar. Mass transfer and species separation due to oscillatory flow in a brinkman medium. *International Journal of Engineering Science*, 74:35–54, 2014.
- [56] G Degan, S Zohoun, and P Vasseur. Forced convection in horizontal porous channels with hydrodynamic anisotropy. *International Journal of Heat and Mass Transfer*, 45(15):3181–3188, 2002.
- [57] Karin G Stenkula and Charlotte Erlanson-Albertsson. Adipose cell size: importance in health and disease. *American Journal of Physiology-Regulatory, Integrative and Comparative Physiology*, 315(2):R284–R295, 2018.
- [58] Sharat C Prasad and Kumbakonam R Rajagopal. On the diffusion of fluids through solids undergoing large deformations. *Mathematics and Mechanics of Solids*, 11(3): 291–305, 2006.
- [59] Gordon S Beavers and Daniel D Joseph. Boundary conditions at a naturally permeable wall. *Journal of Fluid Mechanics*, 30(1):197–207, 1967.
- [60] I P Jones. Low reynolds number flow past a porous spherical shell. In *Mathematical Proceedings of the Cambridge Philosophical Society*, volume 73, pages 231–238. Cambridge University Press, 1973.
- [61] Timir Karmakar and G P Raja Sekhar. Squeeze-film flow between a flat impermeable bearing and an anisotropic porous bed. *Physics of Fluids*, 30(4):043604, 2018.
- [62] Antony A Hill and Brian Straughan. Poiseuille flow in a fluid overlying a porous medium. *Journal of Fluid Mechanics*, 603:137–149, 2008.
- [63] S Tsangaris and E Leiter. On laminar steady flow in sinusoidal channels. *Journal of Engineering Mathematics*, 18(2):89–103, 1984.

- [64] SP Khor, Haig Bozigian, and Michael Mayersohn. Potential error in the measurement of tissue to blood distribution coefficients in physiological pharmacokinetic modeling. residual tissue blood. ii. distribution of phencyclidine in the rat. *Drug Metabolism and Disposition*, 19(2):486–490, 1991.
- [65] George A Truskey, Fan Yuan, and David F Katz. *Transport phenomena in biological systems*, volume 2. Pearson New Jersey, 2010.
- [66] Kerstyn Comley and Norman A Fleck. A micromechanical model for the young’s modulus of adipose tissue. *International Journal of Solids and Structures*, 47(21):2982–2990, 2010.
- [67] Wei Yao, Yabei Li, and Guanghong Ding. Interstitial fluid flow: the mechanical environment of cells and foundation of meridians. *Evidence-Based Complementary and Alternative Medicine*, 2012, 2012.
- [68] Michael J Mueller, Dequan Zou, and Donovan J Lott. “pressure gradient” as an indicator of plantar skin injury. *Diabetes Care*, 28(12):2908–2912, 2005.
- [69] R H M Goossens. Fundamentals of pressure, shear and friction and their effects on the human body at supported postures. In *Bioengineering Research of Chronic Wounds*, pages 1–30. Springer, 2009.